BABAR Analysis Document #183, Version 2.00
July 14, 2001

Vertexing Control Samples

Vertexing and Composition Tools Group [1]

Abstract

The control samples used to monitor the vertexing algorithms and the quality of the data in terms of tracking errors and alignment are described and results based on the Run1 data reported.

[1]Direct contributors to this document are: Bill Dunwoodie (*SLAC*), Carsten Hast (*LAL, Orsay*), Stephen Levy (*U.C. Santa Barbara*), **Fernando Martinez-Vidal (contact person and editor)** (*INFN-Pisa*), Emanuela Pagan (*INFN-Padova*), Eugenio Paoloni (*INFN-Pisa*), Alexis Pompili (*INFN-Bari*) Gerhard Raven (*U.C. San Diego*), Patrick Robbe (*LAPP, Annecy*), Franco Simonetto (*INFN-Padova*), Jan Stark (*LPNHE, Univ. Paris 6&7*), Roberto Stroili (*INFN-Padova*)

Contents

1 Overview

In this document we describe the control samples used to monitor the vertexing algorithms (both single vertex and Δz) and the quality of the data in terms of tracking errors and alignment. Some basic track quality monitoring will be also included soon. Results based on the Run1 data and the different alignment sets are presented.

The vertexing algorithms and techniques used in the control samples here are extensively documented in reference [1].

If you want to have the most up-to-date version you should check-out the head of CVS:

```
% cvs co BAD/note183
% cd BAD
% cvs co pubboard
% ln -s ../pubboard/ .
% latex paper.tex
% ...
```

The majority of the results obtained in this document have been obtained using the *analysis-7* release, otherwise it will be specified.

2 Basic tracking performances

Track parameters, residuals, pulls for Monte Carlo.

Some basic tracking quatities in data: di-muon mis-distance and pull,...

3 $\tau \rightarrow$ 3-prongs

A control sample for vertexing studies have to provide a wide collection of events with a known topology i.e,with a set of tracks coming from the same point.

The τ pairs events in which one τ decays in one lepton and two neutrinos and the other τ decays in three charged particles and a neutrino are ideal for this task in several respects:

- it's possible to select this sample using only vertexing unrelated quantities i.e., events multiplicity, particle identification for the long lived lepton, total energy. The resulting sample is quite pure, the background being at the percent level.
- the sample size is suitable for detailed studies, ($\sim$ 10000 events for an integrated luminosity of one inverse femtobarn).
- the topology is suitable for a complete check of the plain geometric vertexing algorithm.

3.1 Event selection

The details of the selection along to the comparison with the Monte Carlo simulation can be found in references [2] and [3].

We select events with 4 tracks belonging to the *"GoodTracksVeryLoose"* having total charge zero. We require that the stiffest track of the event belongs to the *"MuonLoose"* or *"ElectronLoose"* list and we identify this track as decay product of one τ.

We divide the events in two half-spaces in the center of mass frame defined by the plane perpendicular to the momentum of the stiffest, leptonic track; we require that each half-space contains the decay products of each τ, in turn this implies the requirements:

- neutral energy in the lepton hemisphere lesser than 100 MeV
- momenta of the remaining three tracks belonging to the opposite hemisphere

In order to reduce the contamination from $\gamma\gamma$ events we require that $\sin\alpha > .05$ and $E_{4\pi} > 4\,\mathrm{GeV}$ where

$$\sin\alpha = \frac{|p^T_{tot}|}{E_{cm} - E_{4\pi}}$$

is a variable introduced by the CLEO collaboration which equals the ratio between the modulus of the total transverse momentum p^T_tot , and the missing charged energy $E_{cm} - E_{4\pi}$ using the pion mass hypothesis for all the four tracks, in the center of mass frame.

To reduce radiative Bhabha background we require that no one of the candidates belonging to the 3 prong hemisphere belongs to the *"ElectronTight"* list, that the missing visible energy of the event in the center of mass frame be greater than 1.5 GeV

$$E_{miss} = E_{cm} - E_{4\pi} - E_{neut}$$

where E_{neut} is computed as the sum of the energy of the neutral clusters assuming the photon mass hypothesys in the center of amss frame.

Moreover to ensure a good reconstruction of the event we require that each track owns at least six SVT hits.

The efficiency of this selection is $\sim$ 3.5% and the contamination is order of 2% mainly from continuum *uds* events.

3.2 Control variables

It's possible to build three control variables exploiting the known topology of the events. The strategy is to reconstruct the vertex with a pair of tracks of the three-prong side, and then look at the miss-distances of the remaining track respect to that point. In addition to the miss distance we derived the error on the miss-distances thus being able to check the consistency of the evaluated errors.

The first variable is the miss distance on the transverse plane of the lonely track respect to the pair reconstructed vertex (see fig 1).

$$\delta = d_0 - V_x \sin\varphi_0 + V_y \cos\varphi_0 \tag{1}$$

The second and third variables are the transverse and longitudinal distances (figure 1) of the 3rd track with respect to the vertex defined by the first two tracks, after ordering the tracks by azimuthal and dip angle respectively.

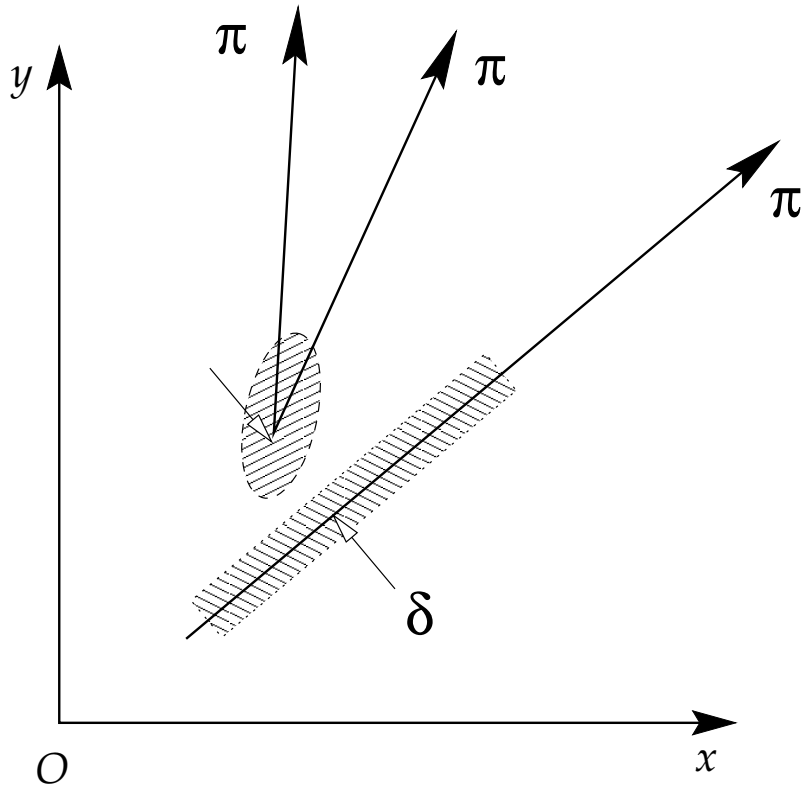

Figure 1: Transverse miss distance from τ events.

3.3 Results

Results for the different control variables are shown in figures 3-10. Table 1 summarizes the most relevant results of this study. Results show that tracking biasese are linked to relative azymuthal/polar angle, and that alignment set E is actually worse than set D. More studies

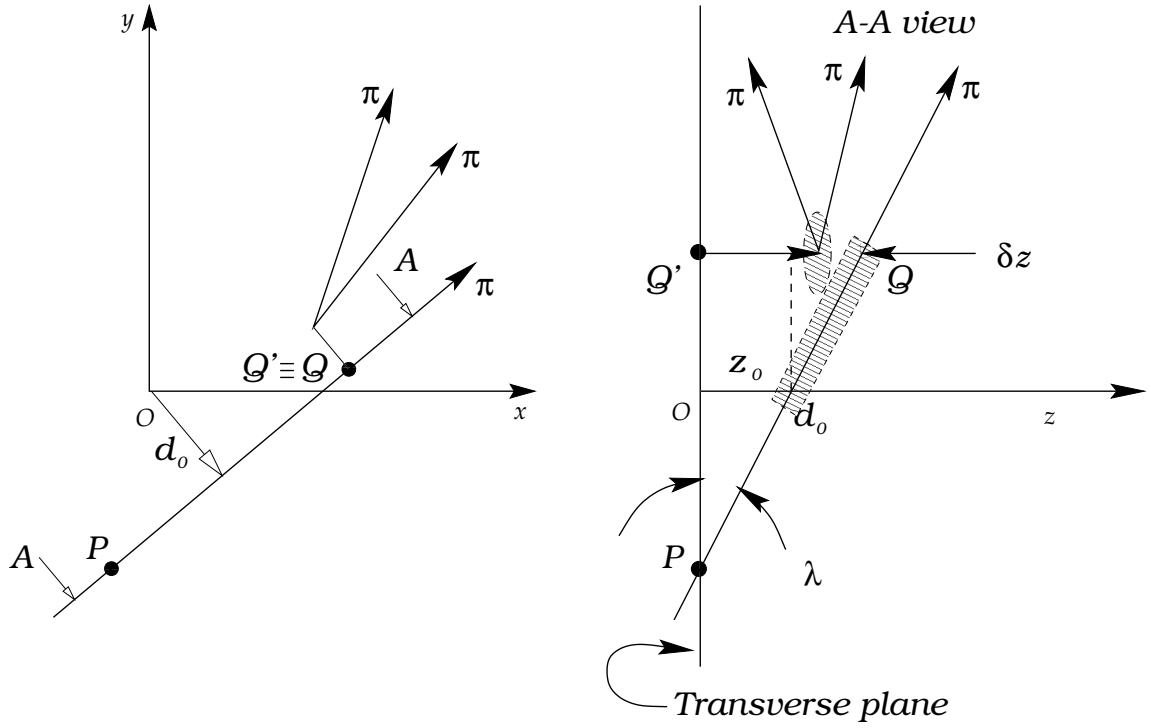

Figure 2: Longitudinal miss distance from τevents.

are under way: i) check newest local aligmnent set (need to recostruct selected tau candidate events), ii) misaligned Monte Carlo studies.

bias	set E	set E	Osaka4 E	Osaka4 D
	μm			
transverse (smallest ϕ)	10.6 ± 1.2	10.1 ± 1.2	12.4 ± 3.5	5.6 ± 4.5
transverse (smallest ϕ) (transverse vertex)	0.3 ± 1.5			
longitudinal forward-most track	22.3 ± 1.5	21.9 ± 1.5	22.0 ± 4.1	9.4 ± 5.3
longitudinal middle dip angle track	1.1 ± 1.2			
longitudinal backward-most track	29.1 ± 1.4			

Table 1: Summary of tracking biases from τ control sample studies.

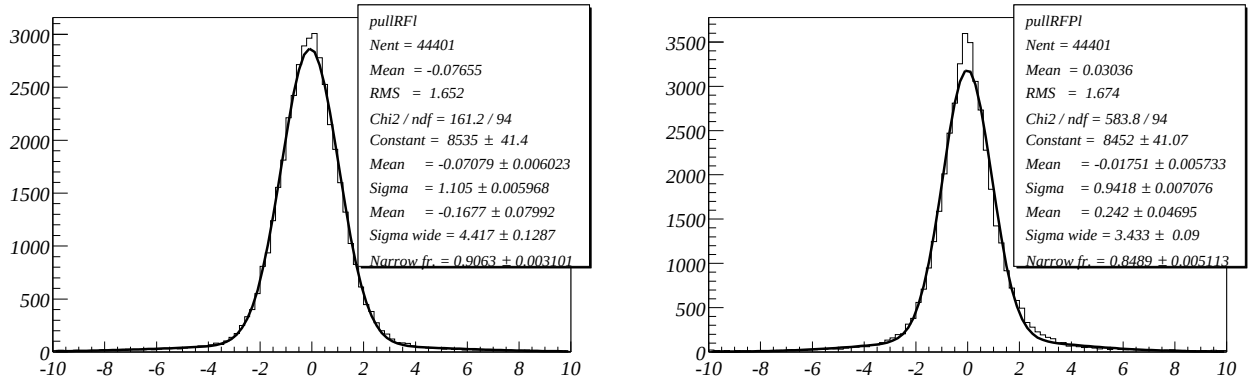

Figure 3: Transverse miss distance pulls for August 2000 and later data, alignment set E, for 3D vertex (left) and vertex done in transverse plane (right).

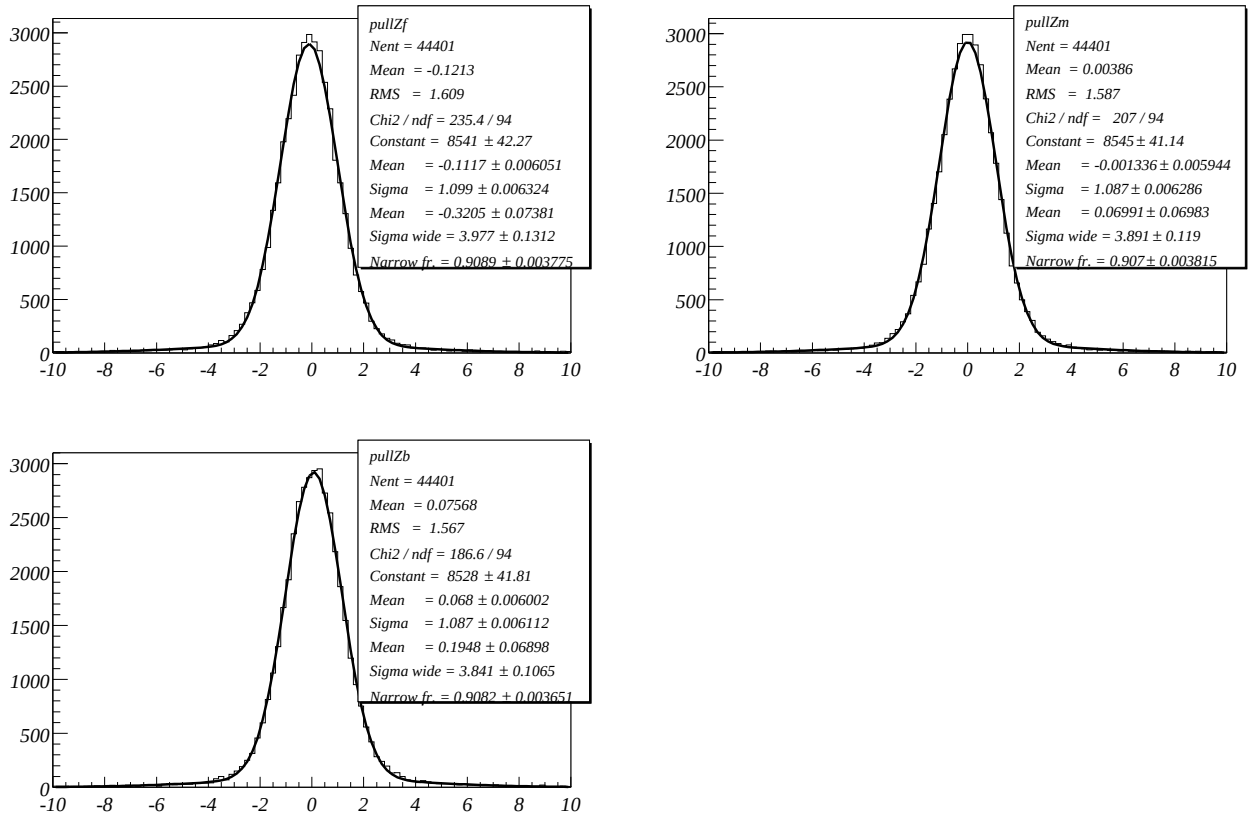

Figure 4: Longitudinal miss distance pulls for August 2000 and later data, alignment set E, for forward track (top/left), mid track (top/right) and backward track (bottom/left).

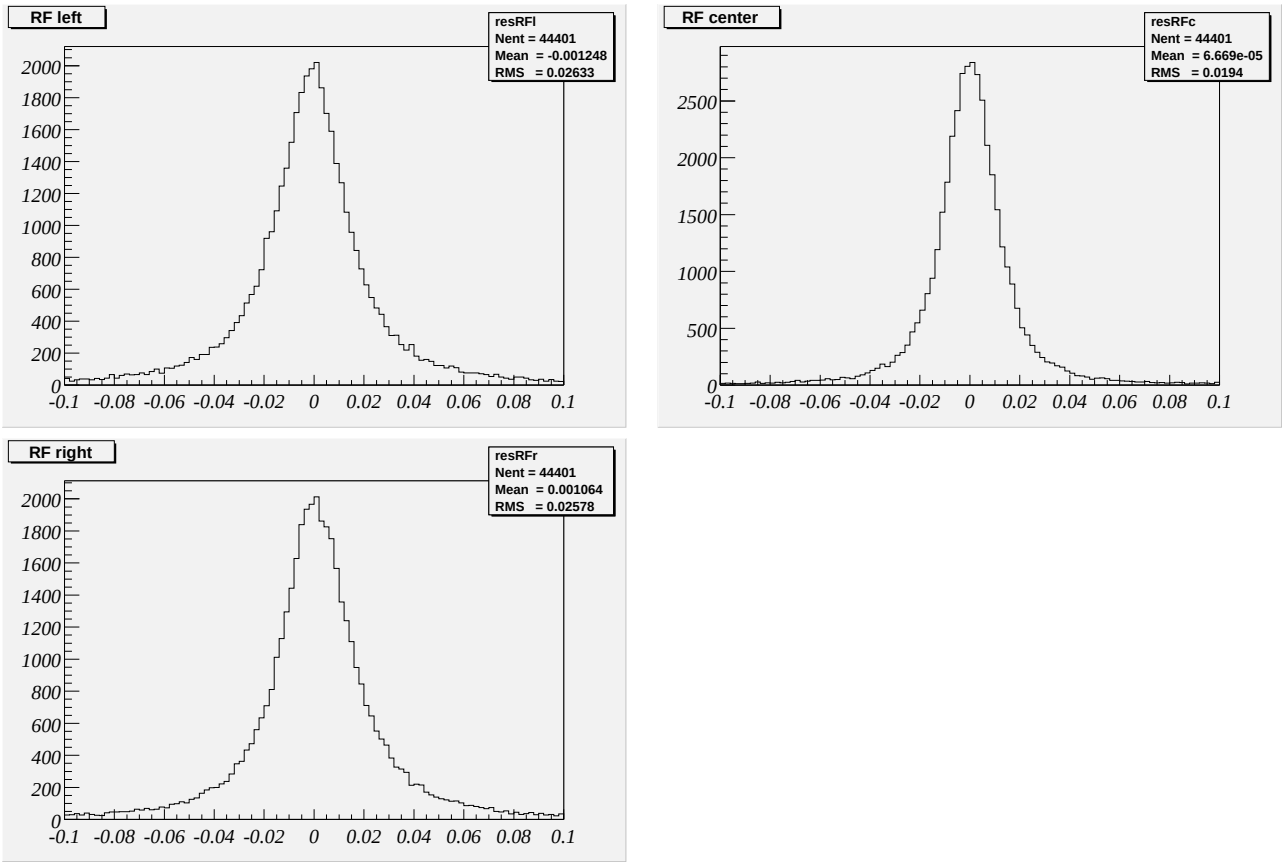

Figure 5: Transverse miss distance residuals for August 2000 and later data, alignment set E, for largest ϕ track (top/left), medium ϕ track (top/right) and smallest ϕ track (bottom/left).

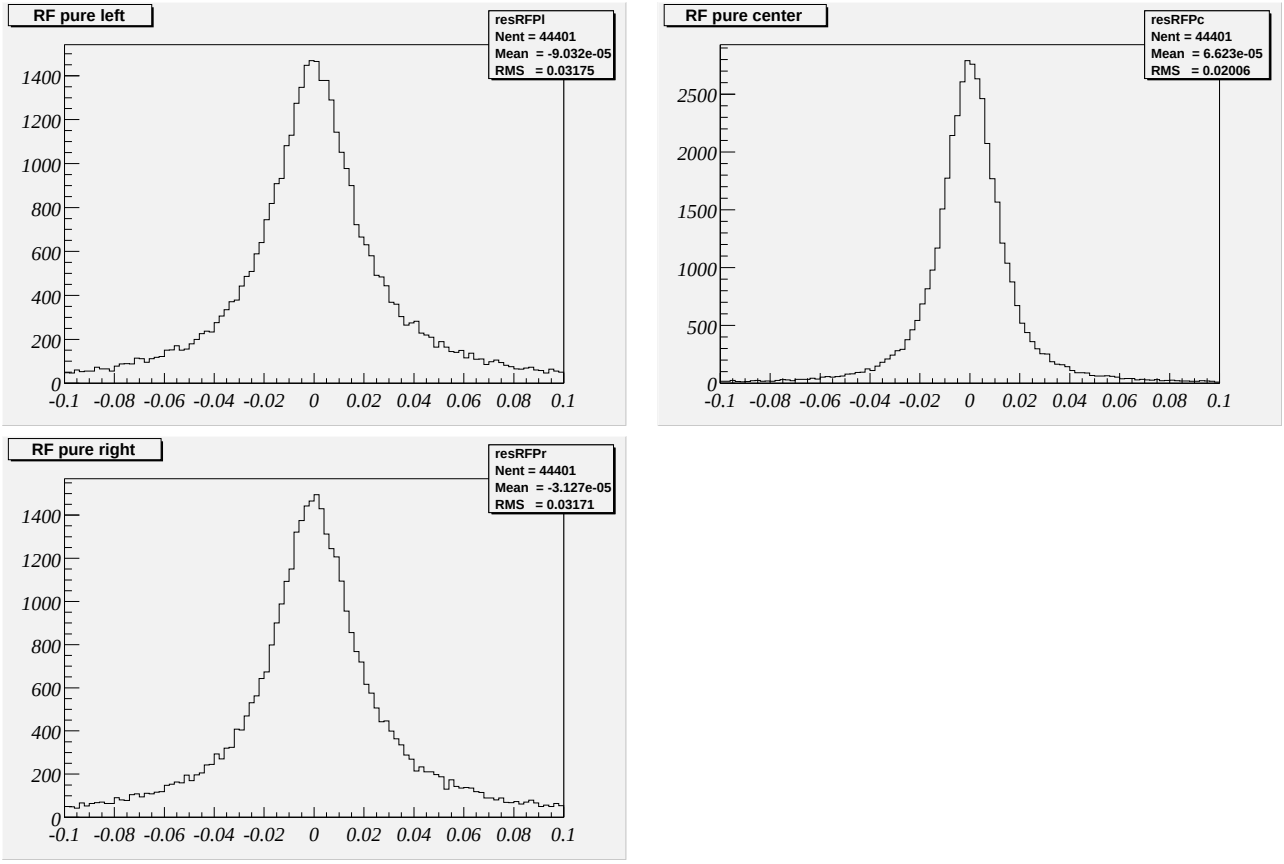

Figure 6: Transverse miss distance residuals for August 2000 and later data, alignment set E, when the vertex has been reconstructed only in the transverse plane, for largest ϕ track (top/left), medium ϕ track (top/right) and smallest ϕ track (bottom/left).

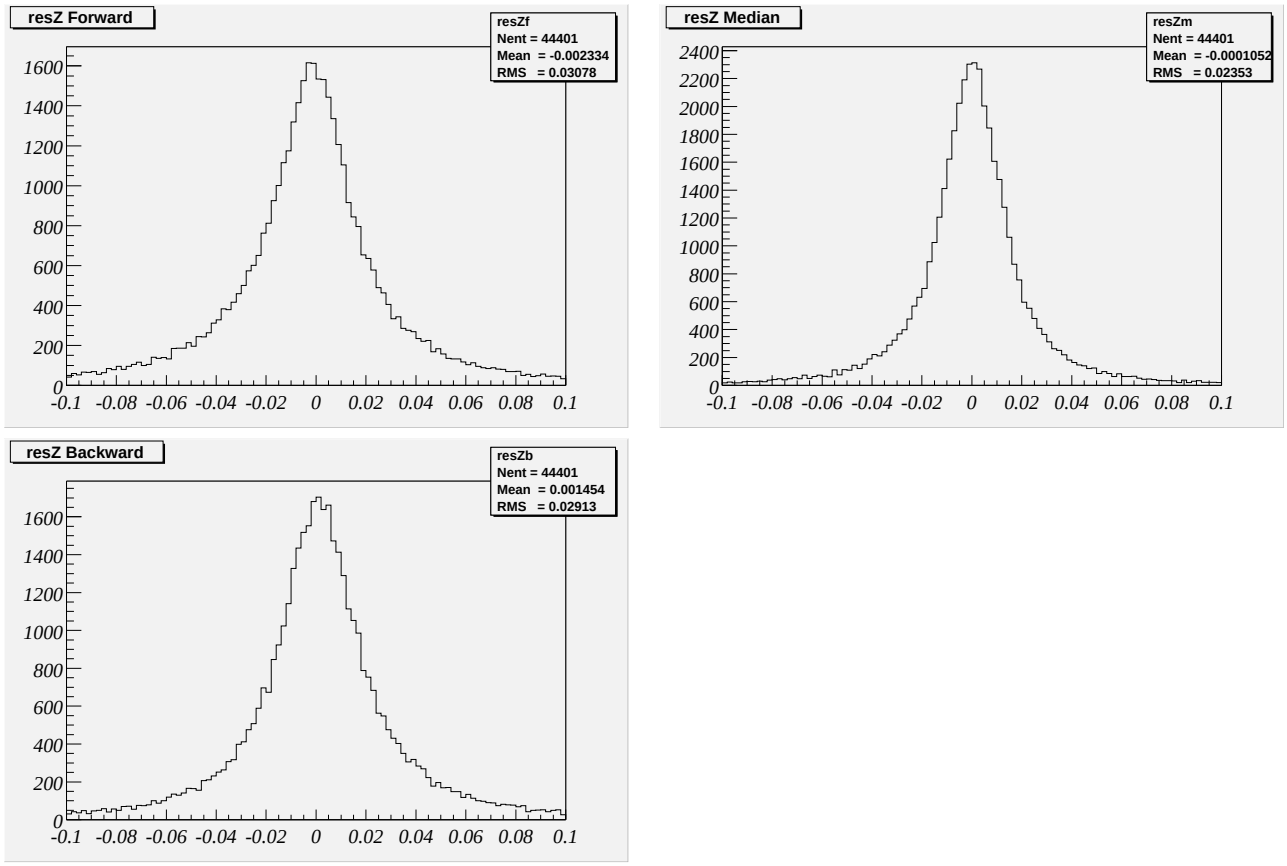

Figure 7: Longitudinal miss distance residuals for August 2000 and later data, alignment set E, for forward-most track (top/left), mid dip track (top/right) and backward-most track (bottom/left).

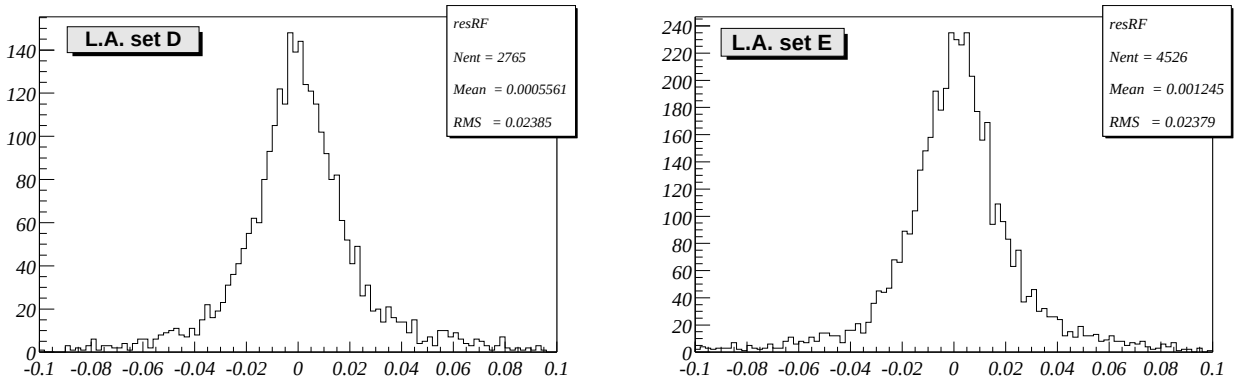

Figure 8: (Left) Transverse miss distance residual, alignment set D, for Osaka-4 data set. (Right) Transverse miss distance residual, alignment set E, for Osaka-4 data set.

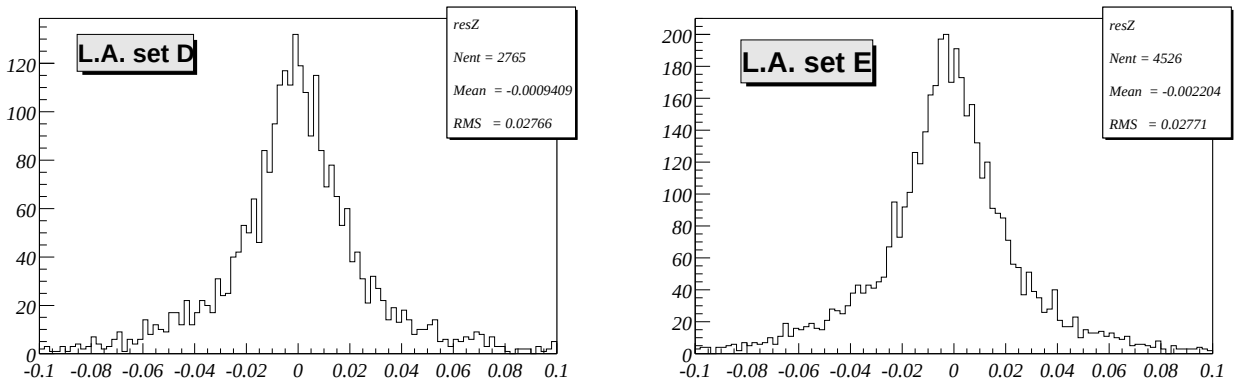

Figure 9: (Left) Longitudinal miss distance residual, alignment set D, for Osaka-4 data set. (Right) Longitudinal miss distance residual, alignment set E, for Osaka-4 data set.

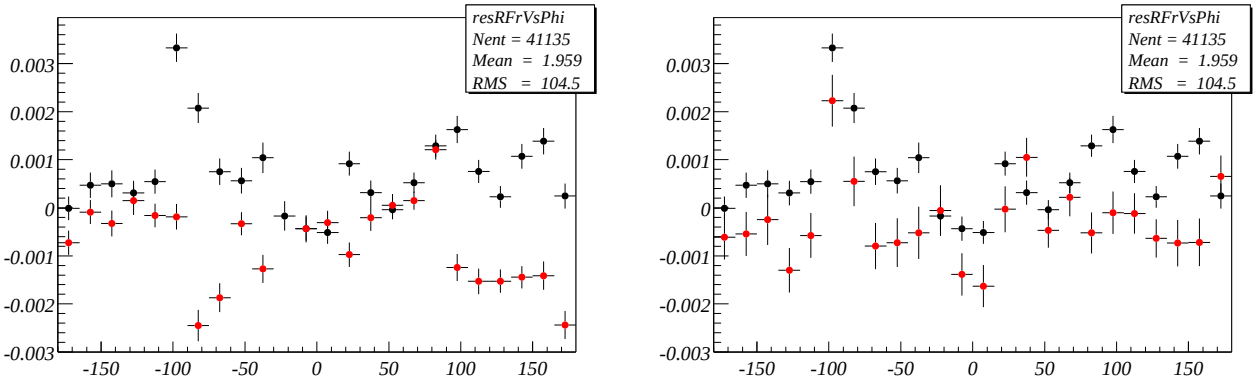

Figure 10: (Left) Transverse average residual as a function of ϕ, alignment set E for largest ϕ tracks (red) and smallest ϕ. (Right) Same but for vertex reconstructed in the transverse plane (read) and in space (black).

4 $D^0 \to K3\pi$

4.1 The $D^0 \to K3\pi$ sample

In the decay process $D^0 \to K3\pi$ four charged tracks are produced from a single space point, corresponding to the position of the D^0 decay. This fact is exploited to determine the resolution in the vertex reconstruction, and compare the Monte Carlo prediction to the real data result, according to the following procedure.

The four particles from the D^0 decay are coupled in two pairs of opposite charge tracks. For each pair a vertex is constructed by intersecting the two particles. Neglecting resolution effects, the two vertices so obtained must then overlap. The distance between the two vertices, projected along the three main coordinates, is then computed event per event, and its spread is interpreted as due only to resolution effects. The pull, defined as the ratio between that distance and its error, is also computed.

Only the events of the so called "Osaka Sample" have been analised. To obtain a good signal to noise ratio, events were selected from the decay chain:

$$\begin{aligned} e^+e^- \to c\bar{c} \to XD^{*+}, \\ D^{*+} \to \pi^+ D^0, \\ D^0 \to K3\pi \end{aligned}$$

(Here and after, the charge conjugate processes are always implied). The event selection is similar to the one applied for the D^0 lifetime measurement. To form the D^0 only tracks from charged particles surviving the following cuts were used:

- a minimum of 8 hit layers in the Silicon Vertex Detector
- a minimum of 20 firing wires in the Drift CHamber
- momentum in the transverse direction $P_t > 70MeV/c$
- distance of closest approach to the main vertex in the $R\phi(z)$ direction less than 1.5 (3.0) cm

The DCH cut was not applied to the soft pion from the D^* decay. D^* and D^0 candidates were retained if they satisfied the further requests:

- $P(D^*) > 2.5$ GeV /c ;
- $P(D^0) > 1.5$ GeV/c ;
- one track tagged as tight kaon by the SMS algorithm with charge opposite to the soft pion ;
- the mass of the candidate D^0 should lie within two sigmas from the PDG value.

(All the momenta are computed in the rest frame). The soft pion track parameters were recomputed after the usual refitting to the beam-spot. The $\delta M = M_{D^{*+}} - M_{D^0}$ distribution for the selected sample is plotted on the left hand side of figure 11 for the real data and on

the right hand side for the simulated events. It should be noted that only pure signal Monte Carlo were employed.

The mass band for the measurement, defined in the range 145.5-146.3 MeV/c^2, contains 16314±127 events. Side bands in the range (140-143.5) MeV/c^2 and (150-155) MeV/c^2 were used for subtraction of the small residual combinatorial background, after proper normalisation.

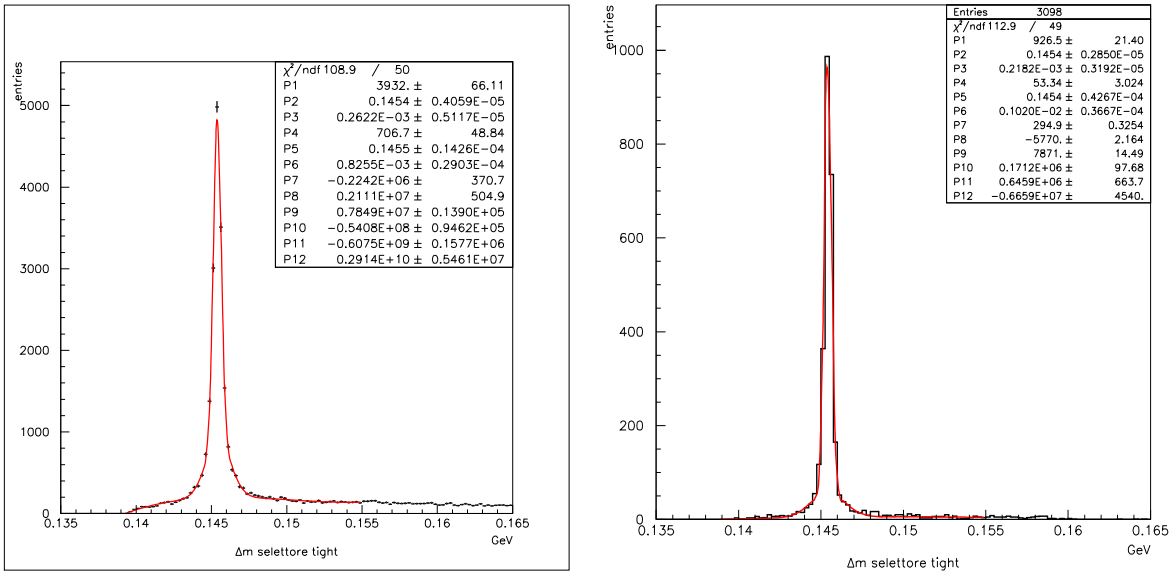

Figure 11: δM distribution for real data events (left) and pure signal Monte Carlo (right). The continuous line in the first histogram shows the sum of the signal distribution, parametrised by the sum of two gaussians, with the fitted combinatorial background.

4.2 Results

The resolution and pull were computed along the three cartesian coordinates. Only the results for the z direction will be quoted here, a more detailed description of the results will be presented in a dedicated note. It should be noted that the conclusions for the z coordinate apply equally well for both x and y.

The resolution for simulated events could be well described by the sum of two gaussians of different width, while the real data exhibited longer tails, and had to be described by the sum of three gaussians (see figure 12 and table 4.2).

The pull distribution for the simulated events can be fitted by a single gaussian, with a width slightly bigger than one. Long tails affect instead the real data pull, which was fitted with two gaussians (see figure 13 and table 4.2): events with big pull values could be either due to bad measurements, or else due to residuals in the background subtraction (see however comments in the conclusions). It should be noted that even neglecting those events the data pull is worse than the one in the simulation: the width of the first gaussian in the data exceeds the simulated one by a factor 1.097±0.020.

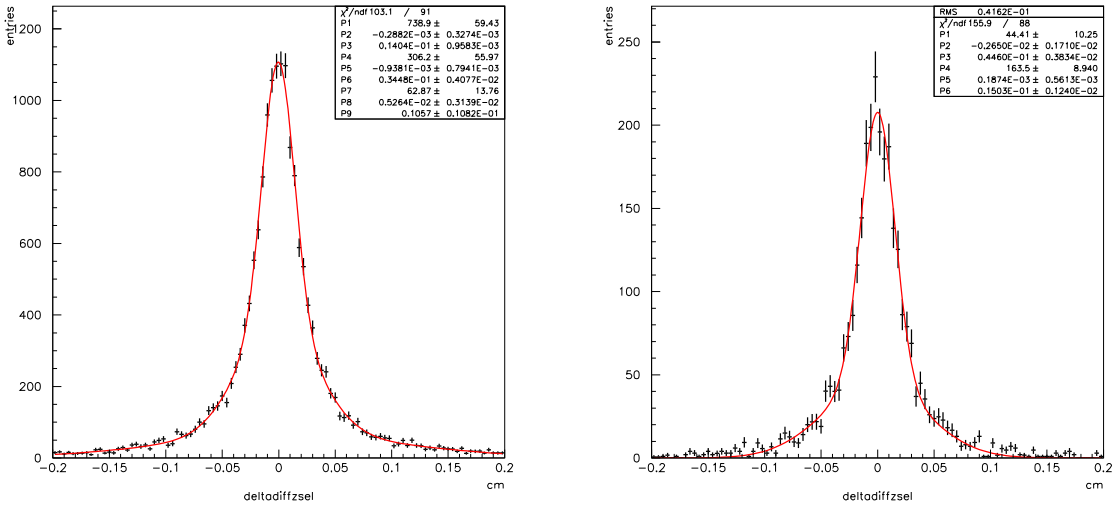

Figure 12: z resolution for real data, background subtracted events (left) and pure signal Monte Carlo (right).

Sample	first		second		third		rms
M.C.	150±12	(55)	450±38	(45)	-		350
data	140±10	(38)	340±40	(38)	1060±100	(24)	516

Table 2: RMS width (μm) of the two (three) gaussians describing the Monte Carlo (real data) z resolution. To ease data-Monte Carlo comparison, the overall RMS width is also reported. The numbers within brackets show the percent fraction of events contained in each gaussian.

Sample	first	second	rms
M.C.	1.075±.017	-	
data	1.179±.008	45.±1.	1.47

Table 3: Pull width of the (two) gaussian(s) describing the Monte Carlo (real data). The overall RMS width for the data is also reported.

4.3 Conclusions and Checks

Events from the Monte Carlo simulation show a RMS z resolution of about 300 μm, and a pull width slightly bigger than one. Real data events have a bigger RMS width ($\sim 500\mu m$) and very wide tails in the pull, which has a RMS width of about 1.5. The real data pull has a core width of 1.179±0.008, exceeding the simulated one by a factor of about 1.1.

Several investigations have been performed to understand the data-Monte Carlo discrepancy:

- Subtraction of combinatorial: the Monte Carlo study was performed on a pure signal

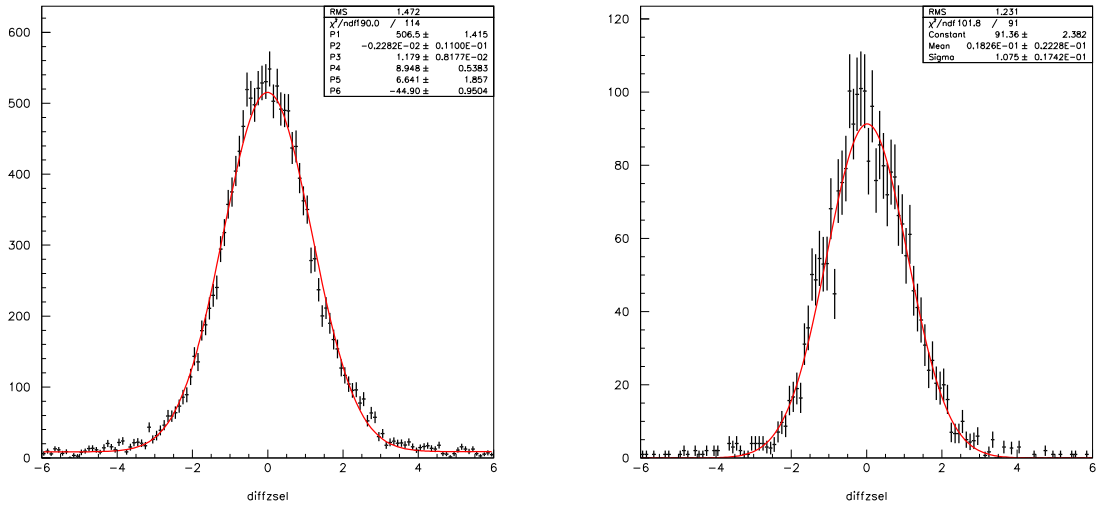

Figure 13: z pull for real data, background subtracted events (left) and pure signal Monte Carlo (right).

sample, whereas in the data the combinatorial had to be subtracted. Due in particular to the SMS K selector, the background level is however small. The analysis was repeated without any kaon selection and, even if the background increased by a factor of about four, the same pattern was found;

- θ, ϕ dependence. The four tracks from the D^0 decay are produced within a narrow cone, centered about the D^0 direction. The analisys was repeated in the data and in the Monte Carlo in several bins of the D^0 polar angle and azimuth, showing that the discrepancy did not depend on any shaky detector region;

- ordering. Results have been presented for pair of randomly selected opposite charge tracks. Tracks were alternatively combined according to several different criteria (momentum ordering, same charge combinations, ordering according to their polar angle, etc.): in any case, no dependency was observed;

- processing. Events were grouped in six subsets, corresponding to different processing (Osaka 1-6 samples). The pull for each sample was bigger than one, but due to the reduced statistics it is not possible to observe discrepancies between the different sets. Figure 14 shows the rms width of the pull as a function of each individual set;

As a conclusion, no clear source for the discrepancy between the data and the Monte Carlo could be identifed.

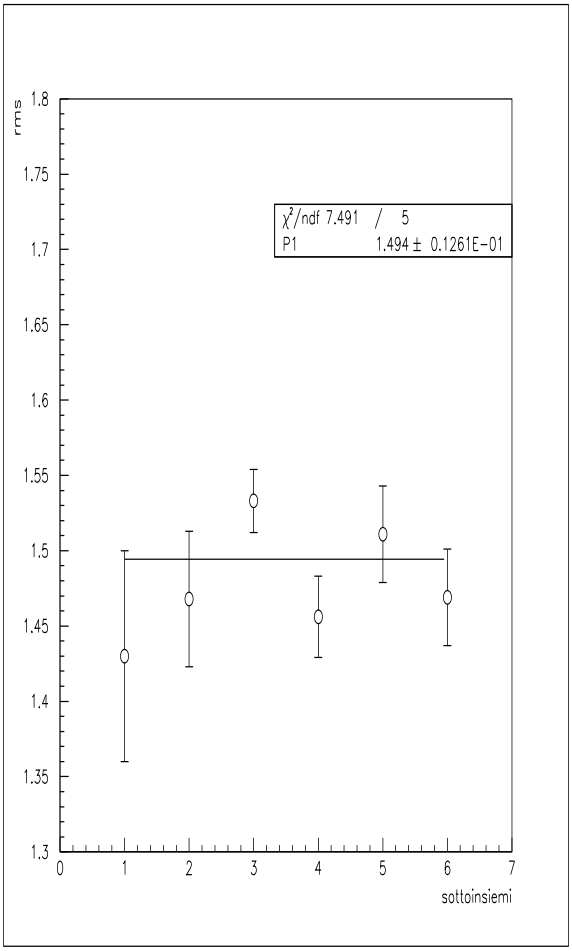

Figure 14: RMS width of the pull distribution, for the six Osaka sets

5 D^0 lifetime in $B^0 \to D^{*-}\ell\nu$ events

The z resolution and scale factor can be estimated from the measurement of the D^0 lifetime in $B^0 \to D^{*-}\ell\nu$ events, since here we have an excelent knowlegde of both the production and decay points. For this check the dedicated $B^0 \to D^{*-}\ell\nu$ vertexing algorithm proposed in [5] and described in [1] is used. This algorithm provides as direct output the D^0 lifetime, taking into account all correlations [1].

The analysis described here (the same presented in [5], it has not been updated since then) makes use of the reduced Kanga files produced from the $B^0 \to D^{*-}\ell\nu$ *expedite skims*, using the `Dstarlnu` package in `analysis-5` release. In the case of multiple candidates per event, the one closest to the nominal D^0 mass is used for analysis. The χ^2 probability of the global fit is well behave, as shown in figure 15.

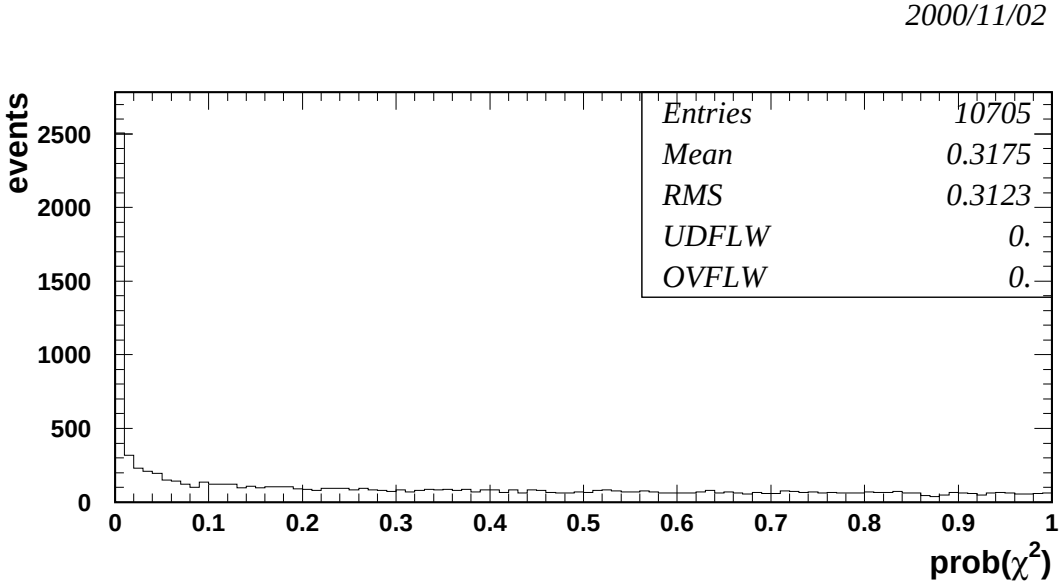

Figure 15: χ^2 probability of the global $B^0 \to D^{*-}\ell\nu$ fit, for data from the *expedite skims*.

The Δm distributions for background and signal regions are shown in figure 16. The Δm for background is fit to a threshold function (independent of event-by-event errors). For signal region, the fit is performed to a double Gaussian with scale factors on event-by-event errors, and separate biases. The results of these MINUIT fits are given in table 5.

No attempt has been done yet to combine the Δm with the lifetime fit. For the time being (and for a while) we cut on Δm and then fit the lifetime, ignoring background. As a consequence, the lifetime result cannot be interpreted yet as the D^0 lifetime, but it is expected that the scale factor will not be significantly affected by the small background component. Figure 17 shows the D^0 decay time distribution together with the result of the fit. The D^0 lifetime is clearly visible. The results of the fit are given in table 5. From this table it can be seen that the scale factor for the core Gaussian is

$$S_{core} = 1.32 \pm 0.03 \ ,$$

and for the tail

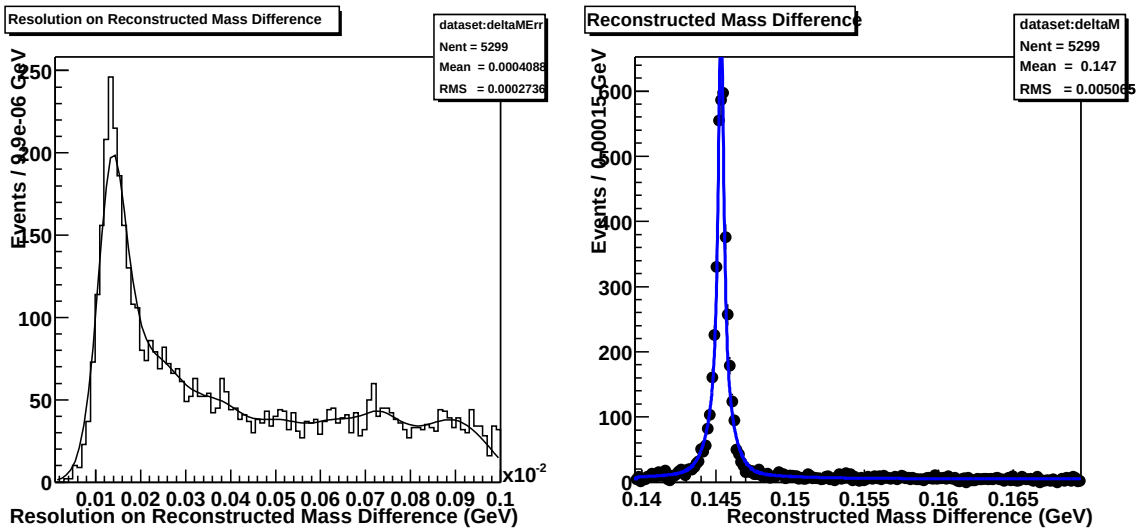

Figure 16: Δm distributions for background (left) and signal (right) regions.

Parameter	Result	Error
piPlusMass	1.39570e-01	constant
c0	7.35229e-05	7.93523e-05
deltaM1	1.45344e-01	5.68368e-06
sfac1	1.19432e+00	2.81013e-02
deltaM2	1.45195e-01	5.28780e-05
sfac2	6.93764e+00	7.10885e-01
fnarrow	7.86960e-01	1.19396e-02
bkgFraction	1.98219e-01	8.46957e-03

Table 4: Δm fit results.

$$S_{tail} = 4.6 \pm 0.3 \ .$$

This analysis still requires some more work:

- add background from D^* sideband fit;
- add background with a real D^*;
- check results in full Monte Carlo;
- compare z and $R\phi$ measurements event-by-event.

It should be note, however, that we don't expect the scale factors be affected significantly by the small backgrounds.

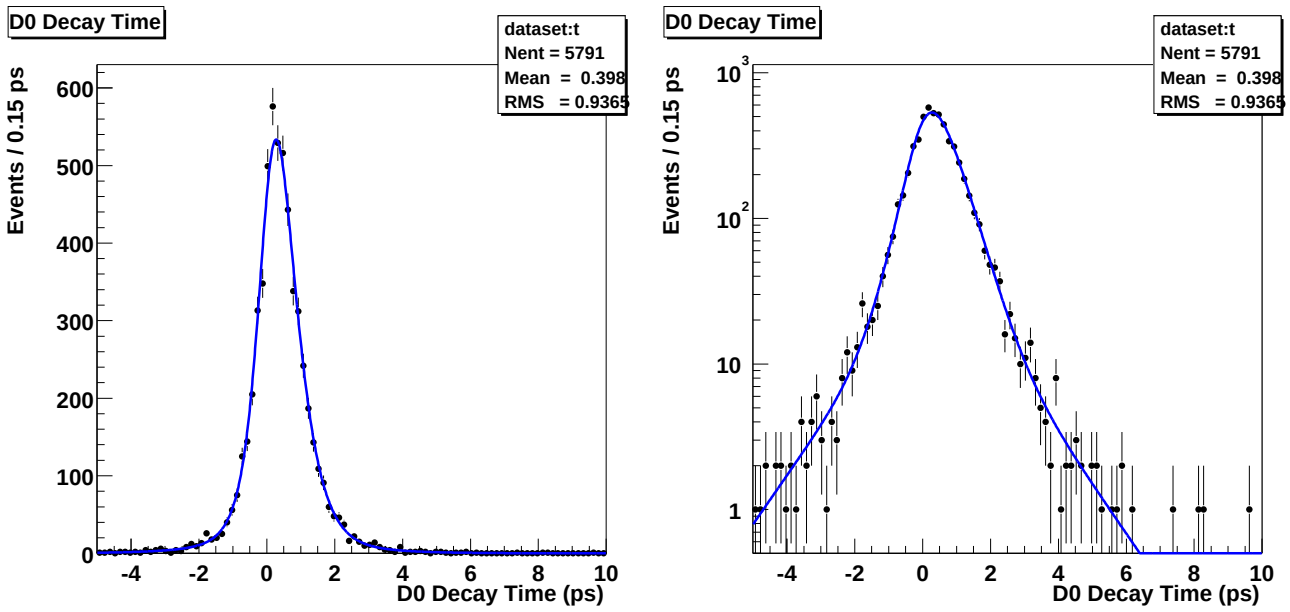

Figure 17: D^0 decay time distribution in linear (left) and logarithmic (right) scales. Superimposed is the result of the likehood D^0 lifetime fit.

Parameter	Result	Error
tauD	3.92765e-01	9.96571e-03
bias1	0.00000e+00	constant
sfac1	1.32272e+00	3.04539e-02
nfrac	8.90333e-01	1.32564e-02
bias2	0.00000e+00	constant
sfac2	4.63012e+00	2.64365e-01

Table 5: D^0 lifetime fit results.

6 $\gamma\gamma \to$ 4-prongs

Alexis

7 Δz control samples

Our knowledge of the resolution function in the data comes out from from the lifetime and mixing analyses. In those fits it is difficult to desintangle the effects of the lifetime and the detector resolution because the width of the observed Δz distribution is the result of the combined widths of the lifetime and the detector resolution, i.e. the information necessary to separate the two effects is in the form of the distribution. As a consequence the measured lifetime and the parameters describing the resolution function are highly correlated. Comparisons with the resolution function from the simulation are useful, but given this difficulty data/MC discrepancies cannot univocally be attributed to the unperfect simulation of the detector response. This situation is significantly more difficult than when using more standard techniques where the time distribution is extracted by reconstructing the production and decay points: here the width of the negative part contains basically only the detector resolution effects, and the positive side is the result of the convolution of the true proper decay time distribution and the detector resultion. Therefore, a detailed understanding of the resolution function in the data, as well as the data/simulation discrepancies is crucial for any analysis using decay length difference techniques. Control samples are therefore an important probe to learn as much as possible from data (and compare to Monte Carlo) about the resolution function.

Two, complementary, control samples has been defined and used to monitor the Run1 data. The first one uses continuum events, the second one uses fully reconstructed D^* mesons from $c\bar{c}$ events. They are described in the following.

7.1 Δz control sample using continuum events

In this study, the charged tracks from off-resonance continuum events are randomly split into two lists. Each list is separately vertexed using `VtxTagSelBtaFit`. Recall that the resolution on Δz is dominated by the resolution of the tag side vertex. Comparing the z-vertex positions from the two lists for data and MC yields a direct measurement of the B_{TAG} resolution in a sample similar but not identical to CP events.

The pseudo-track constraint is not used in the vertexing since the jets are not fully reconstructed. The events are required to have at least 8 charged tracks (guaranteeing that each list is vertexed with at least 4 tracks), an R2 less than 0.6, and are vertexed using the beam spot constraint. Figure 18 shows the comparison between data and MC for the error, χ^2 , probability of the χ^2 , and the number of degrees of freedom of the fit for the z-vertex of one of the lists. Note that there is good agreement for the error on a vertex which is a direct input to the CP asymmetry fit. We also make comparisons between data and MC for Δz of the two lists and a pull which is Δz divided by the errors in quadrature for the vertices. Figure 19 shows the comparison of the resolution and pull on a log scale. We fit the resolutions and pulls to the standard double gaussian plus outlier gaussian. The width of the outlier gaussian for the resolution is fixed at 800 μm and the width of the outlier gaussian for the pull is fixed at 8 sigma. Table 6 shows the comparison of the fit parameters of the resolution and pull for data and MC. The RMS for data and MC are different by approximately 15% for both the resolution and pull.

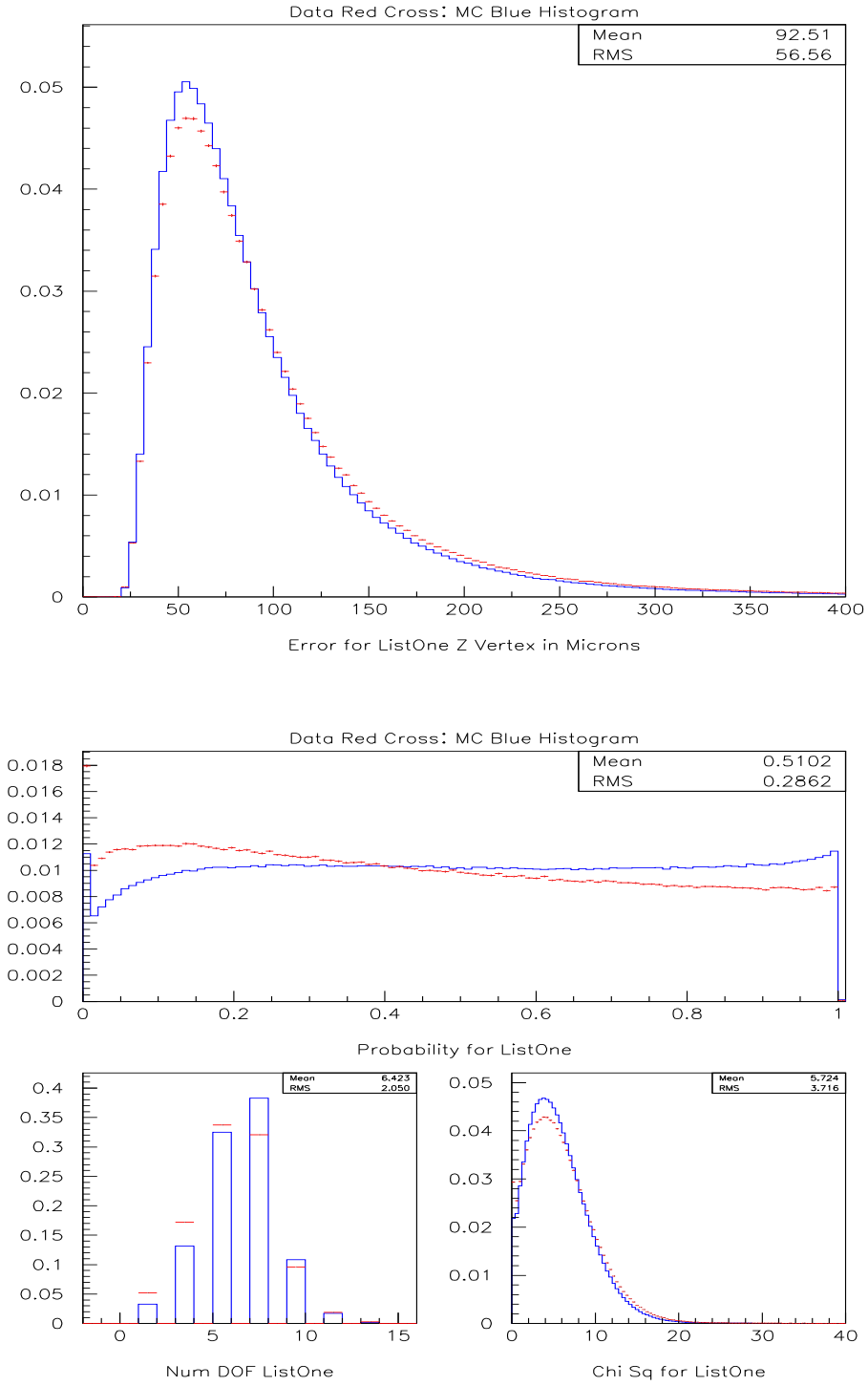

Figure 18: Comparison of the error, χ^2 , probability of the χ^2 , and the number of degrees of freedom on a taglike vertex between data (red cross) and MC (blue histogram).

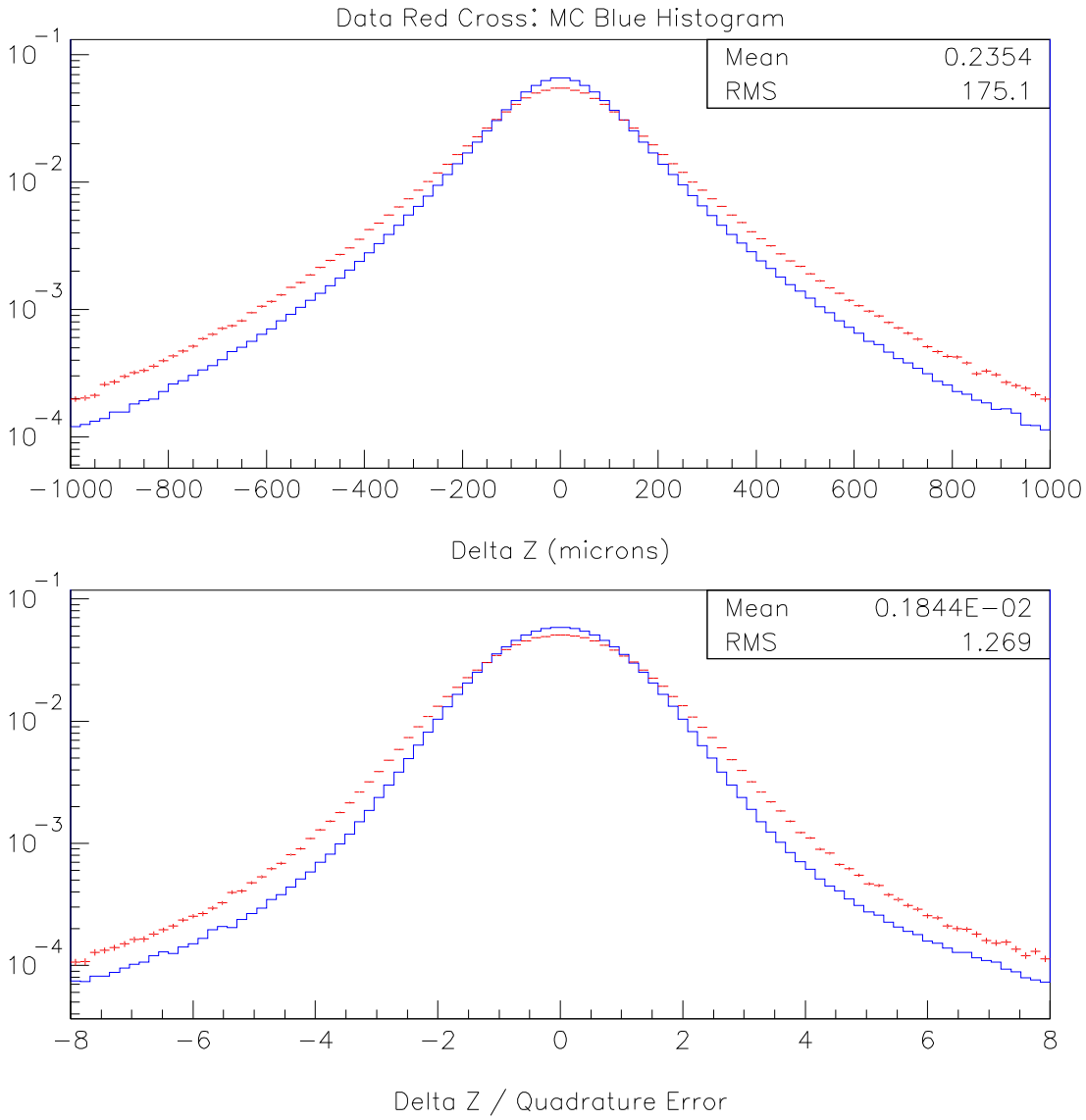

Figure 19: Comparison of Δz, and the pull (Δz divided by the quadrature error of the vertices) for data (red cross) and MC (blue histogram) on a log scale.

Δz reso	f_1	σ_1	μ_1	f_{out}	$\frac{\sigma_2}{\sigma_1}$	$\mu_2 - \mu_1$	RMS	μ
MC	43.3	85. ± 0.2 μm	-0.20± 0.10 μm	11.2	2.09± 0.00	0.61± 0.23 μm	141.± 1. μm	0.10 μm
Data	34.8	96. ± 0.6 μm	-0.35± 0.23 μm	15.6	2.04± 0.01	0.79± 0.45 μm	162.± 1. μm	0.09 μm
Δz pull	f_1	σ_1	μ_1	f_{out}	$\frac{\sigma_2}{\sigma_1}$	$\mu_2 - \mu_1$	RMS	μ
MC	70.0	0.96 ± 0.00	0.00± 0.00	3.88	1.59± 0.01	0.01± 0.00	1.14± 0.01	0.00
Data	55.9	1.06 ± 0.01	0.00± 0.00	6.05	1.55± 0.01	0.00± 0.01	1.32± 0.02	0.00

Table 6: Resolution function parameters for data and MC continuum fits.

7.2 Δz control sample using D^* events

For the selection of this control sample, fully reconstructed D^* mesons from $c\bar{c}$ events are used. The topology of the control events is sketched on Figure 20. Having set aside the tracks from the fully reconstructed D^*, the remainder of the event (fragmentation tracks + charm prongs) can be sujected to the vertex tag algorithm, in this case the default one `VtxTagBtaSelFit` with default configuration (i.e. beam constraints). One expects to find a no flight distribution smeared with a resolution function which mimics that for Δz in B$\bar{\text{B}}$ events. Fragmentation tracks mimic here the prompt tracks in B events.

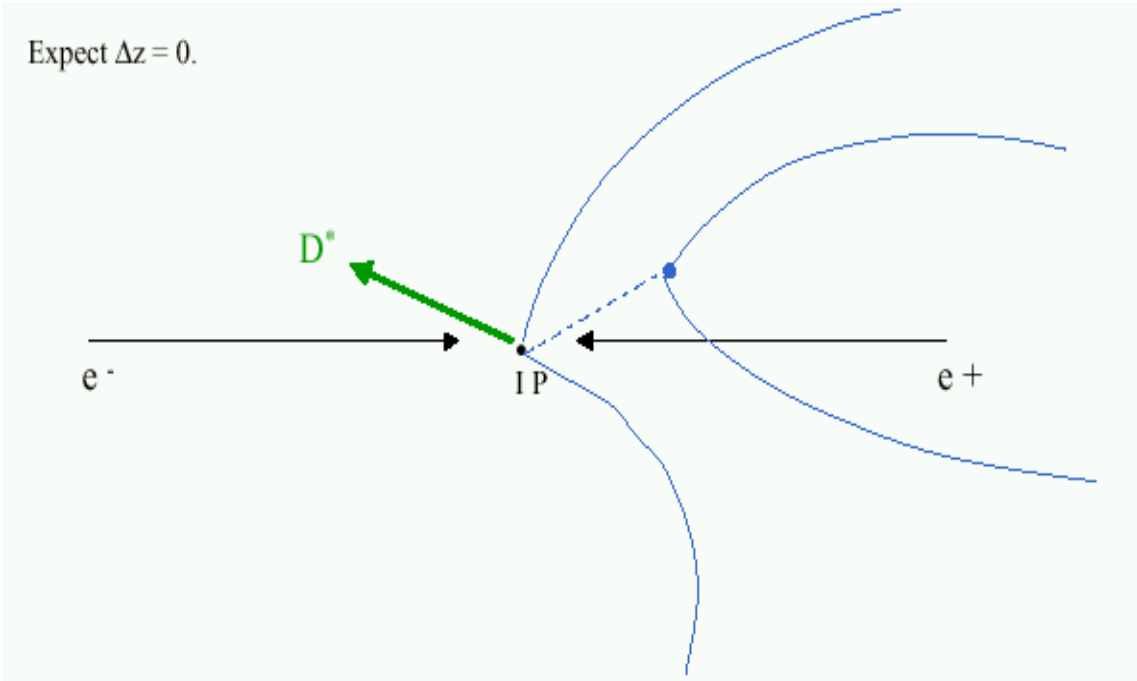

Figure 20: Topology of the events in the control sample.

As fragmentation tracks have a softer spectrum than prompt tracks from B decays, tracks from secondary decays will have higher weight, so it is expected that the resolution function will be in this case slightly more asymmtric and bias biased than for B events. This introduces differences between the resolution function in D^* and B events. However, this feature can be exploited to check how well the Monte Carlo simulation reproduces the charm bias observed in the data. The softer spectrum of the fragementation tracks will be

somewhat compensated by the harder spectrum of tracks from secondary decays, so it is not expected large differences in resolution among both samples. In any case, it is not the purpose of the control sample to provide the resolution function to be used for B physics analysis but rather to have a simple method, as close as possible to the real B events, to make comparisons between the data and the Monte Carlo, for both the resolution and the scale.

The $D^{*+} \to D^0\pi^+$ selection is rather standard:

- $K-\pi^+$, $K^-\pi^+\pi^0$ and $K^-\pi^+\pi^-\pi^+$ modes;
- $p^*(D^0) > 3$ GeV/c;
- D^0 mass within 3 standard deviation of the per-candidate mass error;
- beam spot soft pion refitting, assuming a beam spot width in y of 10 μm;
- $D^{*+} - D^0$ mass difference within 3 standard deviation of the mass difference resolution, taken as 500 KeV/c;
- use *standard* SMS kaon selector for $K-\pi^+$ mode, and *very tight* for $K^-\pi^+\pi^0$ and $K^-\pi^+\pi^-\pi^+$;
- when there are multiple candidates per event, take the one with the best D^0 mass pull (with respect to the PDG mass).

Figure 21 shows the $D^{*+} - D^0$ mass difference spectra (before the $D^{*+} - D^0$ mass cut) for on-peak and off-peak Run1 data, for all modes together. A high statistics and very clean signal is observed.

Figure 22 shows a comparison for B and D^* events obtained from Monte Carlo for some relevant variables: the number, momentum and polar angle of tracks used in the opposite vertex. It can be seen that the distributions are very similar, being the most important difference, as expected, the mean value of the momentum spectra: about 600 MeV for B events and about 1 GeV for D^*'s.

In order to obtain a sample of selected D^* events with a topology as close as possible to that of B events, a $\cos\theta_{D^*} < 0$ cut (where θ_{D^*} is the polar angle of the reconstructed D^*) has been tried. The effect of selecting backward going D^* events on the previous variables has been investigated and results are shown in figure 23. There is an important change in the distribution of the polar angle distribution of the tracks, being it now significantly different from that of B events. Therefore, in the following results this cut has not been used.

Figures 24 and 25 show, respectively, the residual and pull distributions obtained for $c\bar{c}$ Monte Carlo (left) and data (right) D^* events, when beam constraints are applied to the reconstruction of Δz. The superimposed fit was performed using two Gaussians with free bias and width together with an outlier component with 0 bias and 1.3 mm and 8.0 fixed widths for the residual and pull respectively. Figures 26 and 27 are the equivalent distributions without the beam constraints applied to the Δz algorithm, but still applying the beam spot constraint to the reconstruction of the vertex of the D^*. Table 7 summarizes the results of the fits for data and Monte Carlo. They are also ilustrated in figures 28 and

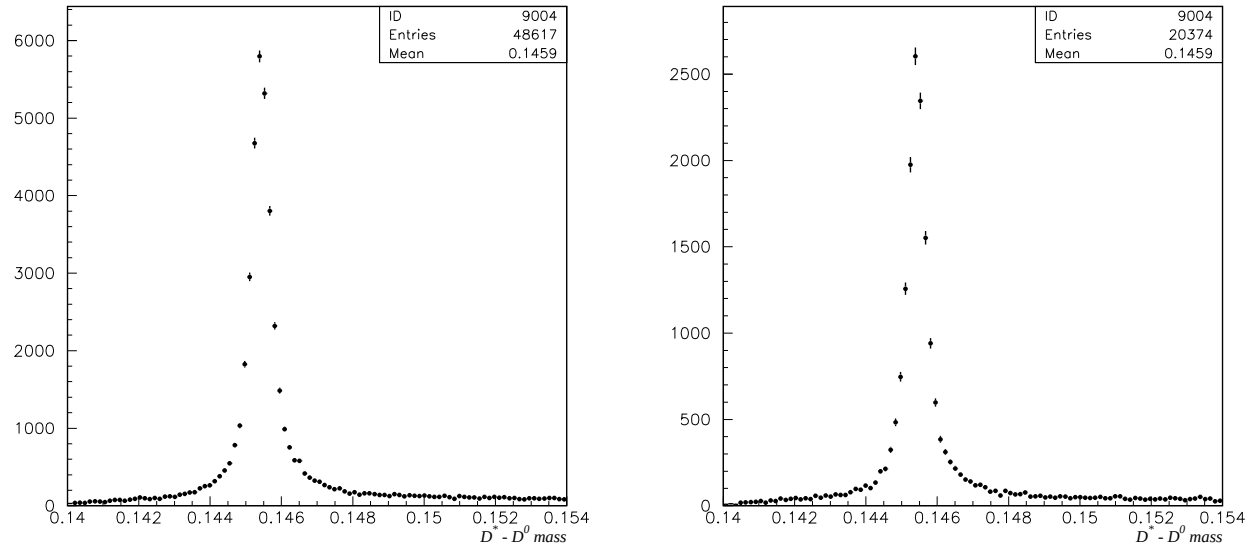

Figure 21: Δm mass difference between the D^* and the D^0 for on-peak (left) and off-peak (right) resonance data.

29, with and without beam constraints, respectively. The fitted resolutions are compared to that predicted by the simulation for $B^0 \to J/\psi K^0_S$ events.

From these figures and table, several interesting points should be noted:

- the resolution in the no beam configuration is significantly worse than that with constraints applied to the Δz algorithm. RMS resolutions are, respectively, 200 and 160 μm, to be compared to about 190 and 170 μm as typically we have for B events, in Monte Carlo;

- the corresponding resolutions in the data are, respectively, about 230 and 170 μm, i.e. $\approx 15\%$ and 10% worse than the Monte Carlo prediction;

- the event-by-event errors provide a good estimation of the resolution;

- there is a 15% pull RMS disagrement between data and Monte Carlo for both, total RMS and central Gaussian, independent wether beam constraints are or are not used;

- charm biases are reasonably well reproduced by the Monte Carlo. It is interesting to note that, contrary to what one naively would expect by similarity with the B events, biases are here larger in the configuration where beam constraints are applied. This can be explained by the fact that when selecting D^* events from $c\bar{c}$ continuum, the extrapolation to the 'other side' implied by the pseudo-track mechanism will select predominatly tracks around the recoiling jet. As fragmentation tracks are uniformly distributed, this mechanism favors the selection of charm prong tracks, in the same way that in B events it favors B prongs. It would be interesting to rerun the sample

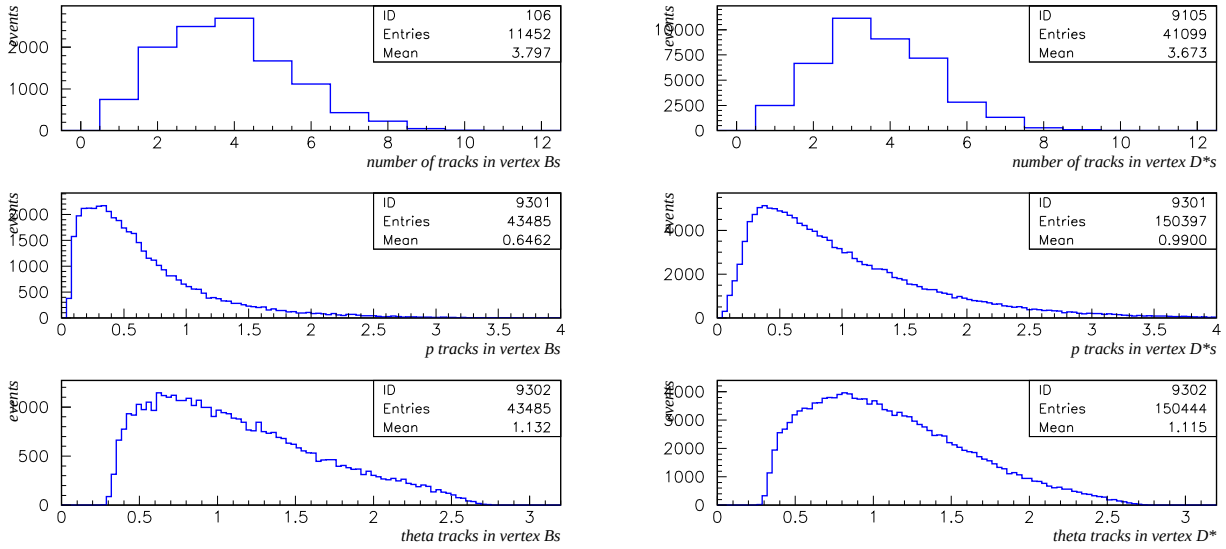

Figure 22: Number, momentum and polar angle of tracks used in the vertex tag for B (left) and D^* (right) events from continuum in Monte Carlo.

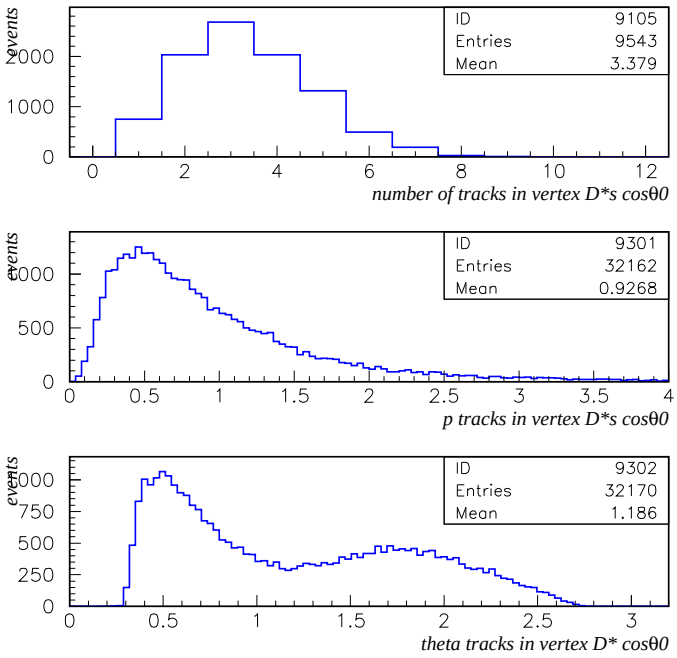

Figure 23: Number, momentum and polar angle of tracks used in the vertex tag for backward going selected D^* events.

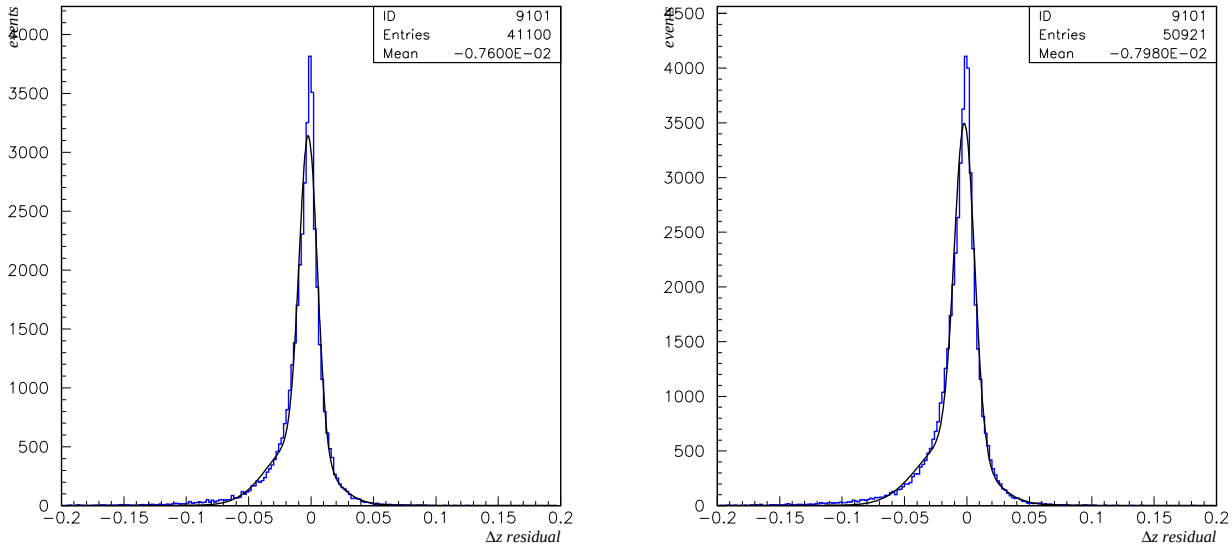

Figure 24: Δz residual distributions for (left) $c\bar{c}$ Monte Carlo and (right) data (right) D^* events when beam constraints are applied.

applying only the beam spot constraint: in this case it is expected the maximum bias reduction, with a resolution similar to what is found with the Δz algorithm in default configuration (beam constraints).

Finally, figures 30 and 31 compare several variables (Δz residual, Δz per-event error, Δz pull, χ^2 probability and number of tracks in the vertex) in data and Monte Carlo for the beam and no beam configurations, respectively. Apart of the differences in resolution and pull between data and Monte Carlo, it is quite striking (for both configurations) the large difference in the shape χ^2 distribution. An important contribution to this disagreement is due to misalignement effects, not included in the Monte Carlo simulation. However, the fact that differences here seem to be significantly larger than those reported for B events [7] seems to indicate that at higher momentum tracking errors are underestimated, what is somehow the contrary of what one would expect from differences in multiple scattering. This effects is currently under investigation.

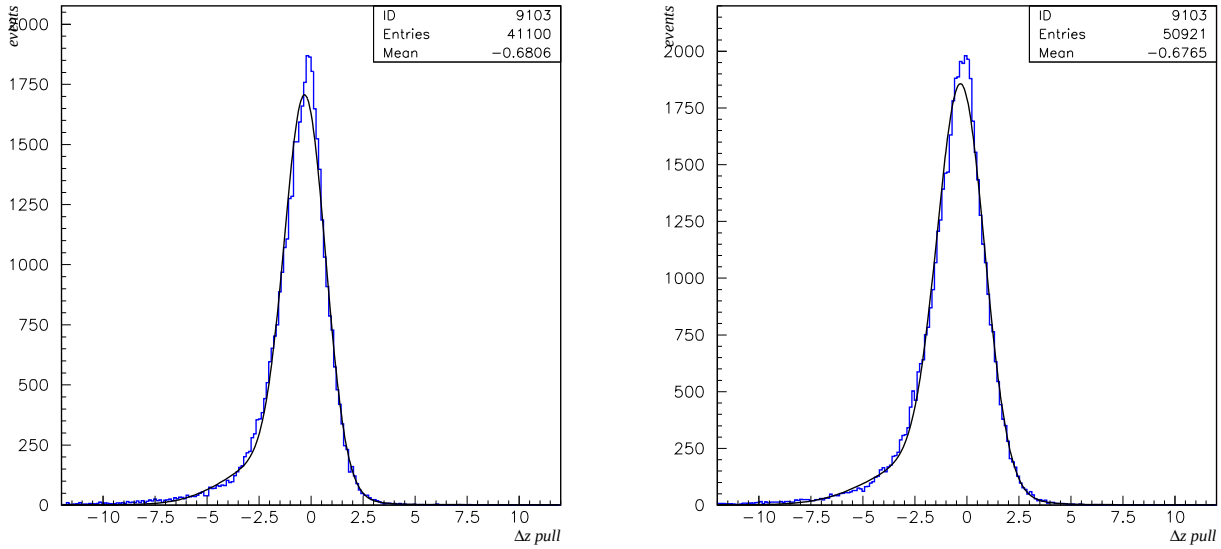

Figure 25: Δz pull distributions for (left) $c\bar{c}$ Monte Carlo and (right) data (right) D^* events when beam constraints are applied.

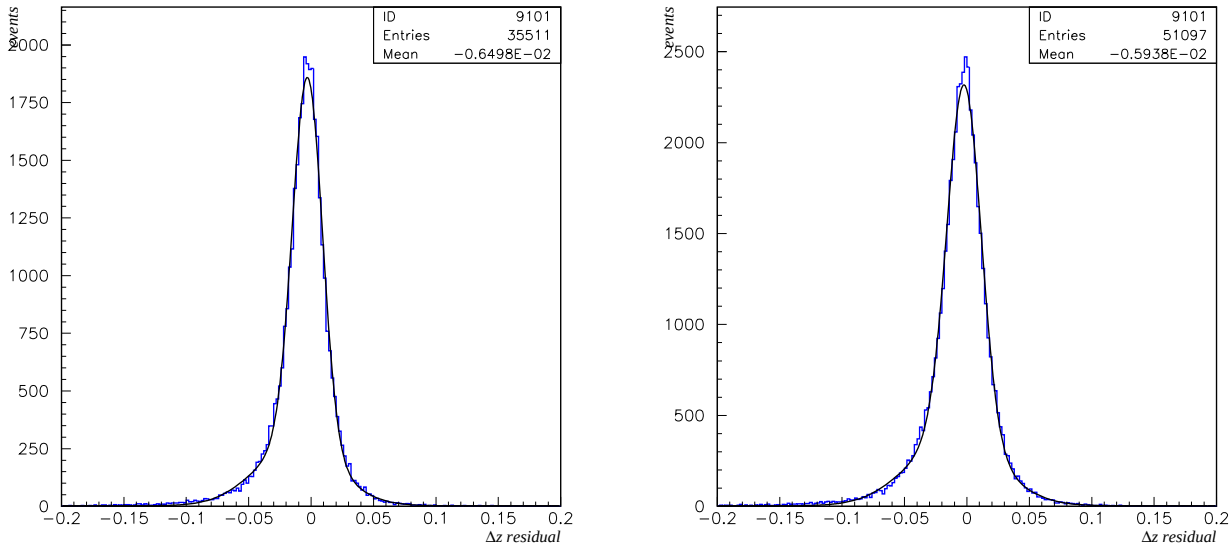

Figure 26: Δz residual distributions for (left) $c\bar{c}$ Monte Carlo and (right) data (right) D^* events without beam constraints.

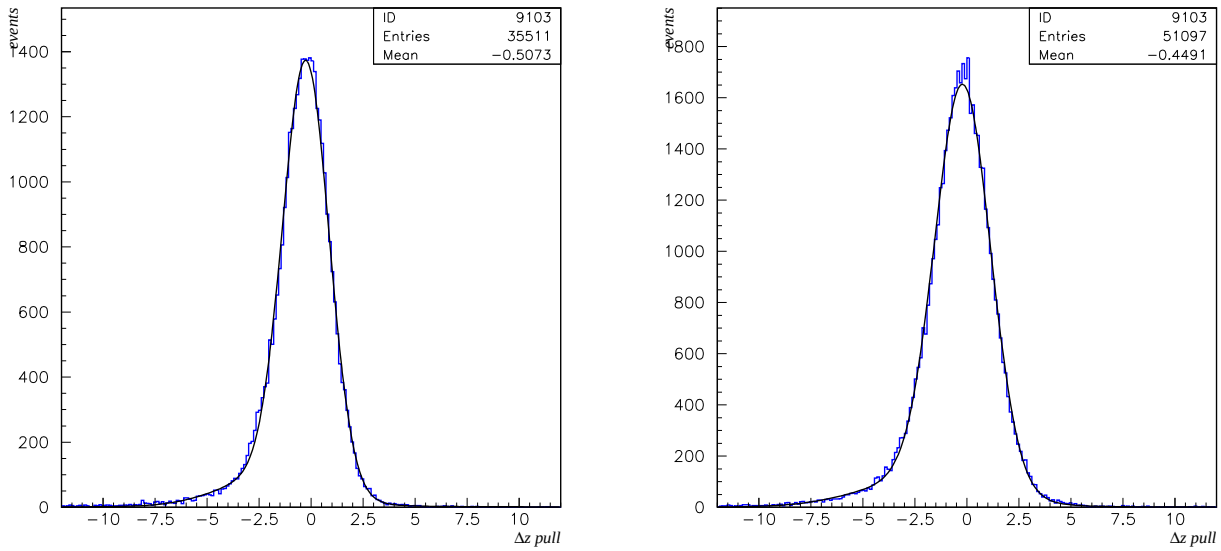

Figure 27: Δz pull distributions for (left) $c\bar{c}$ Monte Carlo and (right) data (right) D^* events without beam constraints.

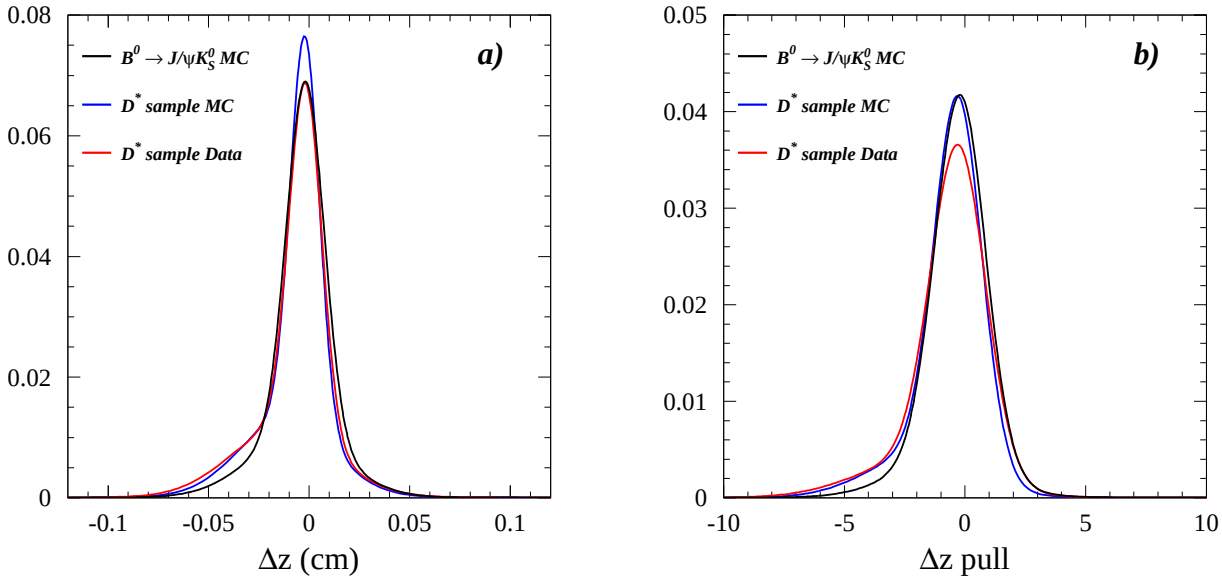

Figure 28: Fitted resolution function for the D^* control sample in data and Monte Carlo, for a) the distance between the D^* vertex and the vertex determined from the rest of the tracks in the event (using beam constraints) and b) for this distance divided by the calculated error on the distance. For comparison, the resolution function for $B^0 \to J/\psi K^0_S$ events in Monte Carlo is shown.

	f_{core}	f_{out}	μ_1	σ_1	μ_2	σ_2	RMS	μ
Δz Residual (μm)								
$c\bar{c}$ MC (with constraints)	0.598 ± 0.008	0.021 ± 0.0012	-21.8 ± 0.7	72.0 ± 1.0	-118 ± 3	232 ± 3	158 ± 2	-61 ± 2
data (with constraints)	0.604 ± 0.007	0.0189 ± 0.0010	-19.5 ± 0.7	80.8 ± 1.0	-132 ± 3	257 ± 3	174 ± 2	-64 ± 2
$c\bar{c}$ MC (without constraints)	0.669 ± 0.012	0.0229 ± 0.0015	-28.2 ± 0.9	118.0 ± 1.5	-116 ± 5	309 ± 6	203 ± 3	-57 ± 2
data (without constraints)	0.645 ± 0.011	0.0196 ± 0.0013	-21.1 ± 1.1	134.5 ± 1.7	-104 ± 4	343 ± 6	231 ± 3	-51 ± 2
Δz Pull								
$c\bar{c}$ MC (with constraints)	0.798 ± 0.010	0.0123 ± 0.0013	-0.286 ± 0.010	0.982 ± 0.010	-1.97 ± 0.08	2.11 ± 0.05	1.30 ± 0.14	-0.63 ± 0.03
data (with constraints)	0.806 ± 0.008	0.0094 ± 0.0012	-0.277 ± 0.009	1.131 ± 0.009	-2.16 ± 0.08	2.43 ± 0.04	1.48 ± 0.14	-0.64 ± 0.03
$c\bar{c}$ MC (without constraints)	0.857 ± 0.009	0.0155 ± 0.0018	-0.245 ± 0.009	1.113 ± 0.010	-1.93 ± 0.11	2.38 ± 0.08	1.37 ± 0.14	-0.50 ± 0.03
data (without constraints)	0.859 ± 0.007	0.0083 ± 0.0015	-0.197 ± 0.009	1.337 ± 0.009	-2.01 ± 0.10	2.95 ± 0.06	1.66 ± 0.14	-0.45 ± 0.03

Table 7: Results from the fits to the Δz residuals and pull in the D^* control sample with and without beam constraints applied to the Δz reconstruction, for $c\bar{c}$ Monte Carlo (on-resonance) and data. The RMS does not include the outlier component.

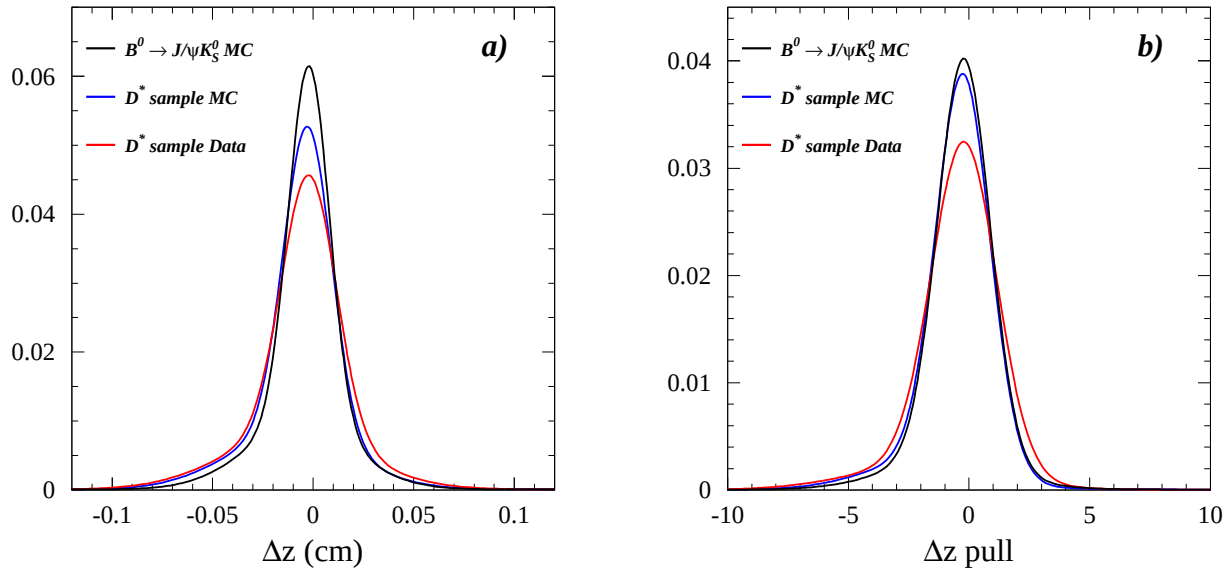

Figure 29: Fitted resolution function for the D^* control sample in data and Monte Carlo, for a) the distance between the D^* vertex and the vertex determined from the rest of the tracks in the event (without beam constraints) and b) for this distance divided by the calculated error on the distance. For comparison, the resolution function for $B^0 \to J/\psi K^0_S$ events in Monte Carlo is shown.

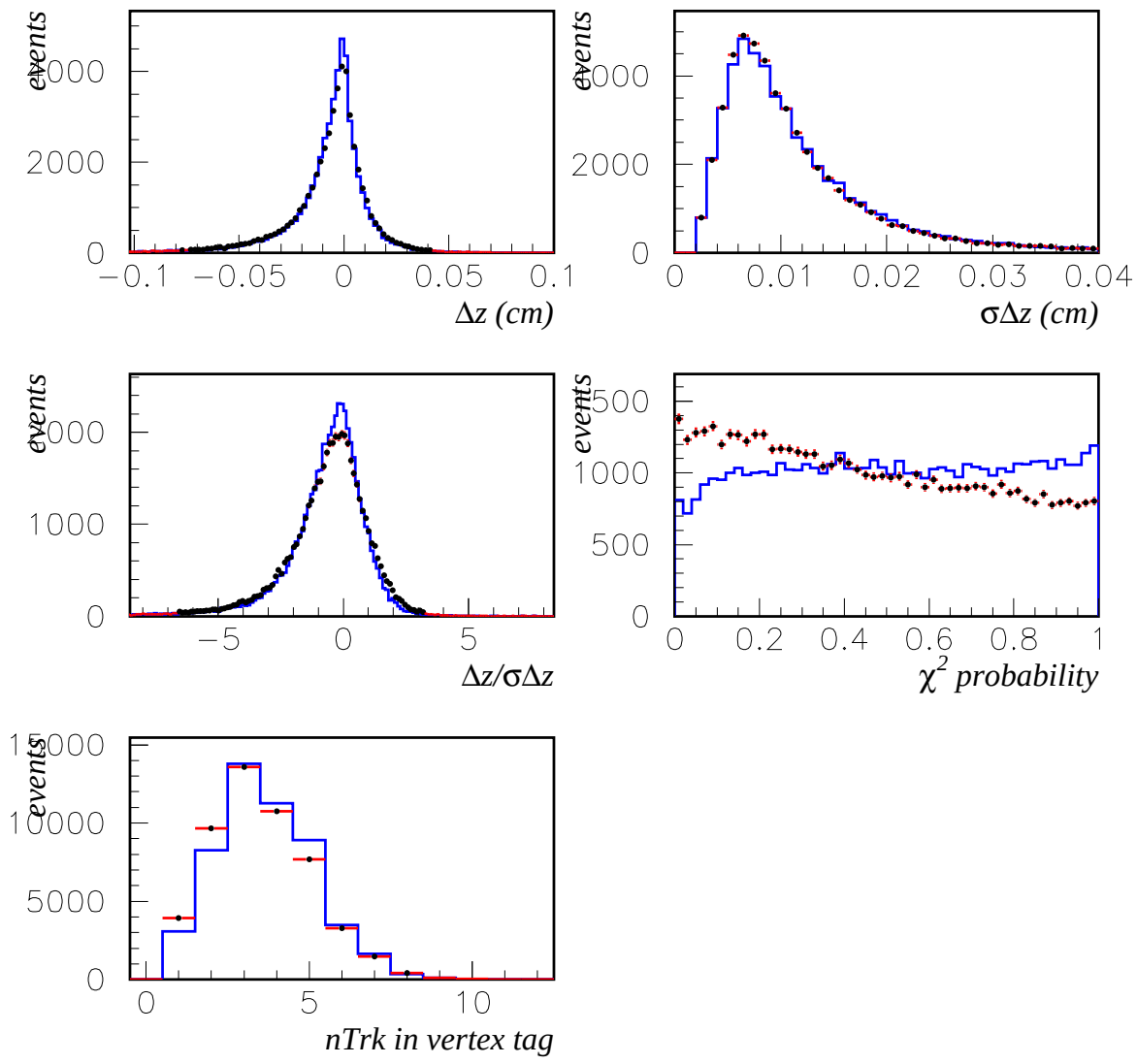

Figure 30: Data/MC comparison of: Δz residual, Δz per-event error, Δz pull, χ^2 probability and number of tracks in vertex, for the D^* control sample when beam constraints are applied.

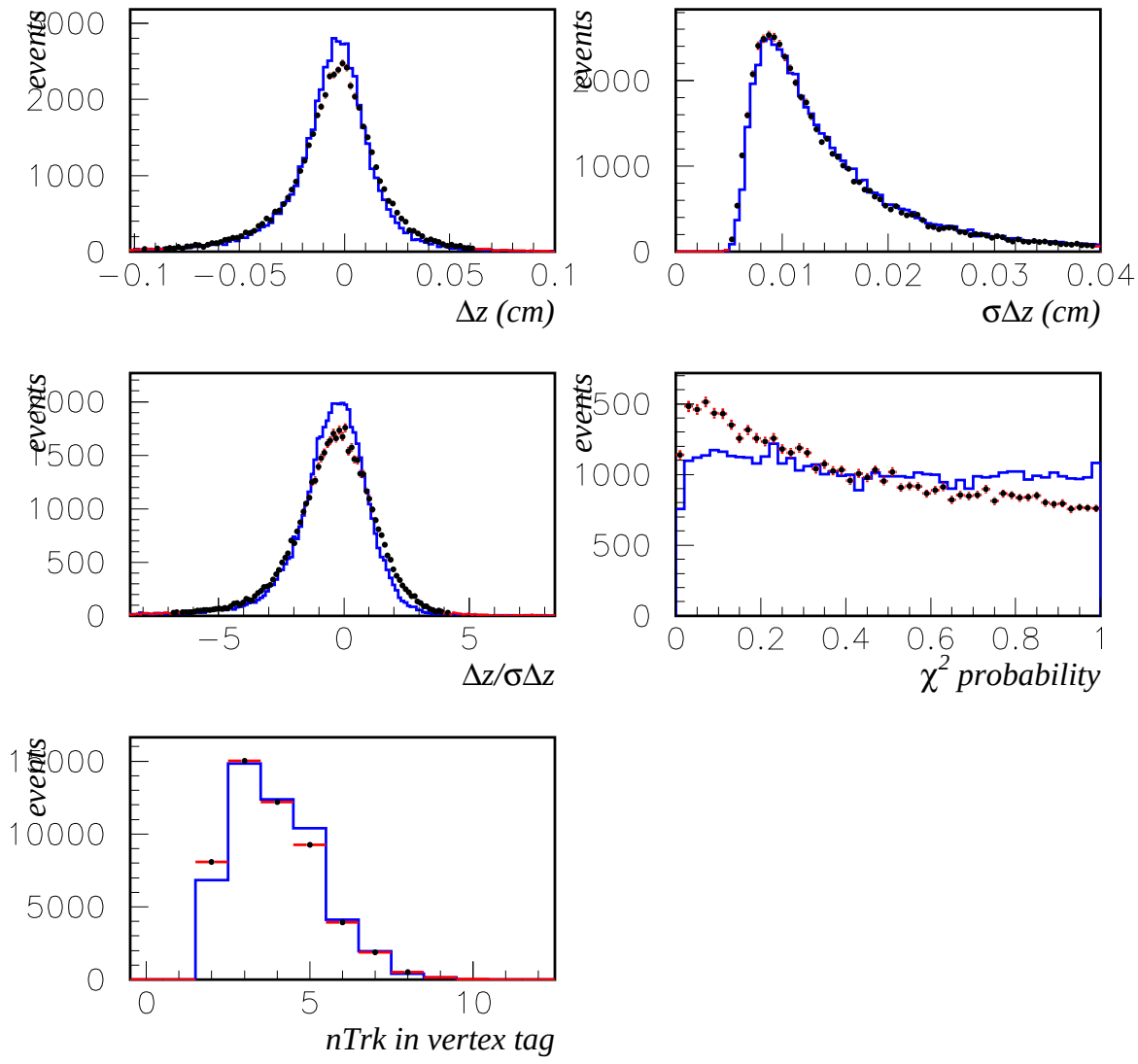

Figure 31: Data/MC comparison of: Δz residual, Δz per-event error, Δz pull, χ^2 probability and number of tracks in vertex, for the D^* control sample without beam constraints.

8 Estimation of the SVT Longitudinal and Transverse Length Scales

The length scales corresponding to the reconstruction of vertices at radii less than that of the innermost SVT layer are relevant to the systematic uncertainties associated with the measurement of τ, charm and B lifetimes. The reconstruction of vertices corresponding to off-beam electroproduction of hadrons in the material of the beampipe allows the possibility of measuring its dimensions to high precision. The comparison of measured and nominal dimensions then yields estimates of the relevant scale values.

8.1 Experimental Procedure

A detailed description of this analysis can be found in reference [6]. Off-beam electroproduction interactions in the material of the B-Factory detector may be characterized by the existence of at least one baryon among the final state positively-charged particles. A global look at dE/dx as a function of momentum for such processes reveals the dominant presence of protons together with some production of deuterons and tritons. In the studies described here, we choose to require the presence of a well-identified proton among the final state particles of the events to be used.

8.1.1 Proton Identification

To identify protons in the *BABAR* detector, the information obtained from two subdetectors is used :

- *Drift Chamber* : measurement of dE/dx,
- *DIRC* : value of the Čerenkov angle.

The comparison with the expected values for a *proton* using the Bethe-Bloch parametrisation contained in the condition database and the theoretical Čerenkov angle value computed with the proton mass enables the selection of protons with high reliability.

8.1.2 Material Interaction Vertices

Once a proton is identified in an event, one or several tracks are vertexed with it. All vertices formed with a χ^2 probability greater than 0.1% using the same proton are compared and that with the highest χ^2 probability is kept.

In order to obtain high precision measurements, the following vertex and track quality cuts are required :

- $\sigma_x < 100\ \mu m$, $\sigma_y < 100\ \mu m$, $\sigma_z < 330\ \mu m$, where σ^2 is the relevant diagonal element of the vertex fit covariance matrix;
- all tracks must have at least 6 hits in the SVT;
- the proton track must have at least 20 hits in the Drift Chamber;

- vertices for which $r < 2\ cm$ are excluded from consideration.

This sample contains Λ decays since this particle has a large flight length ($c\tau_\Lambda = 7.89\ cm$). The vertices associated with Λ decays constitute a background as they can occur at random positions. To remove them an additional cut on the $p\pi^-$ invariant mass is performed and vertices with $mass(p\pi^-)$ in$[1.11; 1.13]$ GeV/c^2 are rejected.

Figure 32 shows the positions in the $x - y$ plane of the reconstructed vertices. Since the structure of the inner detector appears clearly, we are confident that then interaction vertices in the detector material are well-reconstructed.

8.2 Beampipe Geometry

The ruler used for this study is the Beampipe. The measurement of the z locations of the points at each end where the amout of material increases significantly will give an estimate of the z scale factor. The radial material distribution will likewise provide an estimate of the radial length scale.

8.2.1 Longitudinal Structure

The beampipe in essence consists of two Beryllium cylinders with a layer of cooling water in between. The radius of the outer cylinder, the *water jacket*, increases at both extremities of the beampipe. With respect to the Interaction Point, the z coordinates of those two points are :

- $z_{backward} = -78.720\ mm$
- $z_{forward} = +101.370\ mm$

Two layers of Tantalum foil are wrapped around the outside of the water jacket. The foil was aligned to the points where the width of the beryllium changes. Since the interaction rate is much higher in the Tantalum than in the beryllium, our measurment will be sensitive to the position of the Tantalum foil more than to the position of the jumps in the water jacket. For that reason we assign a 200 μm error on the distance between the two points of interest. Then the nominal distance to be measured using material interactions is :

$$\text{distance}_{nominal} = 180.090 \pm 0.200\ mm \tag{2}$$

8.2.2 Radial Structure

8.3 Results

The results presented in this section were obtained using *isPhysicsEvent* collections processed with releases 8.6.3c, 8.6.4b and 8.6.5a in a range of run numbers between 11332 and 12708. This represents a total of 3.4 fb^{-1}. SVT Local Alignment Conditions C were applied to process these runs.

8.3.1 Beampipe Position

As a first step, we must establish the position of the beampipe with respect to the *BABAR* coordinate system. It turns out that the beampipe is indeed rotated and translated with respect to the z axis of the coordinate system. Figures 33 are scatter plots of R versus ϕ in different z regions. The presence of a one period sinusoidal shape on those plots is a confirmation of a shift of the beampipe.

The beampipe rotation and shift parameters are obtained with the following procedure. Each vertex with coordinates (x, y, z) found in the beampipe is rotated and shifted according to :

- x_c, the x coordinate of the center of the beampipe in the $z = 0$ plane,
- y_c, the y coordinate of the center of the beampipe in the $z = 0$ plane,
- $dxdz$, the rotation angle in the $y = 0$ plane,
- $dydz$, the rotation angle in the $x = 0$ plane.

The result of this transformation is a point with coordinates (x', y', z'). A χ^2 value is then calculated as indicated in (3), and is minimized with respect to the four above parameters and R, the mean value of the radius of the beampipe.

$$\chi^2 = \sum_{i=1}^{N} \left(\frac{R - \sqrt{x_i'^2 + y_i'^2}}{\sigma_R^i} \right)^2 \tag{3}$$

The fit is performed with MINUIT and the results are given in table 8.

As a check, after applying those corrections, the R versus ϕ scatter plot of figure 34 does not show any sinusoidal shape.

8.3.2 Absolute z Scale

Figure 35 shows the mean radius versus z profile distribution. The increase of radius at both ends of the beampipe due to the Tantalum foil is clearly visible.

The measurement of the location of each discontinuity will consist in fitting the local mean R versus z distribution using the function $f\,(z; R_1, R_2, z_{step}, \sigma)$ defined in (4).

$$\begin{aligned} f\,(z; R_1, R_2, z_{step}, \sigma) &= (R_1\theta\,(z' - z_{step}) + R_2\theta\,(z_{step} - z')) \otimes g\,(z - z'; \sigma) \\ &= \frac{1}{2}\left(R_1 \mathrm{erfc}\frac{z - z_{step}}{\sqrt{2}\sigma} + R_2 \mathrm{erfc}\frac{z_{step} - z}{\sqrt{2}\sigma} \right) \end{aligned} \tag{4}$$

In this expression, $\theta(z)$ is the Heavyside function, $g(z; \sigma)$ a Gaussian of resolution σ and the fitted parameters are :

- R_1, the left part mean radius,
- R_2, the right part mean radius,

- z_{step}, the position of the step,
- σ, the resolution of the Gaussian.

At each end, a z interval of 5.5 mm centred approximately on the discontinuity is used for the χ^2 fit. The result for each region is shown in figure 36.

The results are as follows :

- $(z < 0)\ z_{step} = -79.583 \pm 0.042\ mm$
- $(z > 0)\ z_{step} = 100.540 \pm 0.085\ mm$

The fitted distance between the two steps is then :

$$\text{distance}_{fitted} = 180.123 \pm 0.095\ mm \tag{5}$$

Using (2) and (5), an estimate of the z scale factor can now be obtained :

$$\boxed{z \text{ Scale Factor } = \frac{\text{distance}_{fitted}}{\text{distance}_{nominal}} = 100.02 \pm 0.12\ \%} \tag{6}$$

8.3.3 Absolute R Scale

8.4 Absolute z Scale for SVT LA Sets C, D and E

Table 9 gives the z Scale factors determined using the method described above for three different SVT Local Alignment Sets.

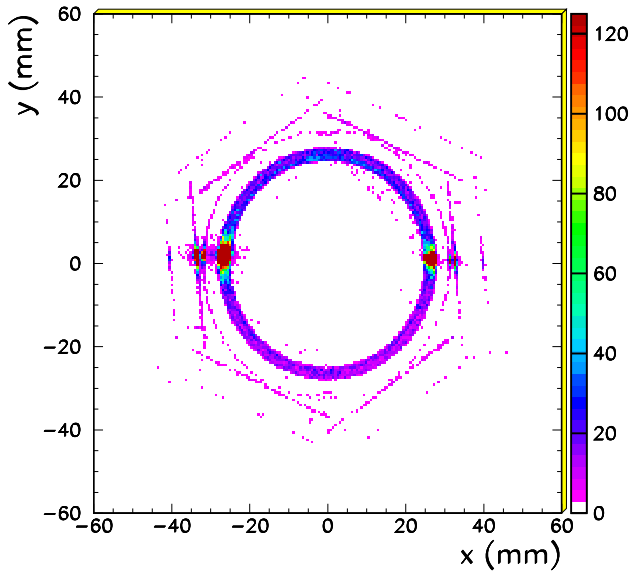

Figure 32: Position of the Reconstructed Vertices in the $x - y$ plane.

Table 8: Beampipe position parameters for Local Alignment Set C

Parameter	Value
x_c	223 μm
y_c	-4 μm
$dxdz$	1.26 $mrad$
$dydz$	-1.51 $mrad$

Table 9: Absolute z Scale for Local Alignment Sets C, D and E

SVT LA Set	Absolute z Scale
C	$100.02 \pm 0.12\%$
D	$99.99 \pm 0.12\%$
E	$100.22 \pm 0.14\%$

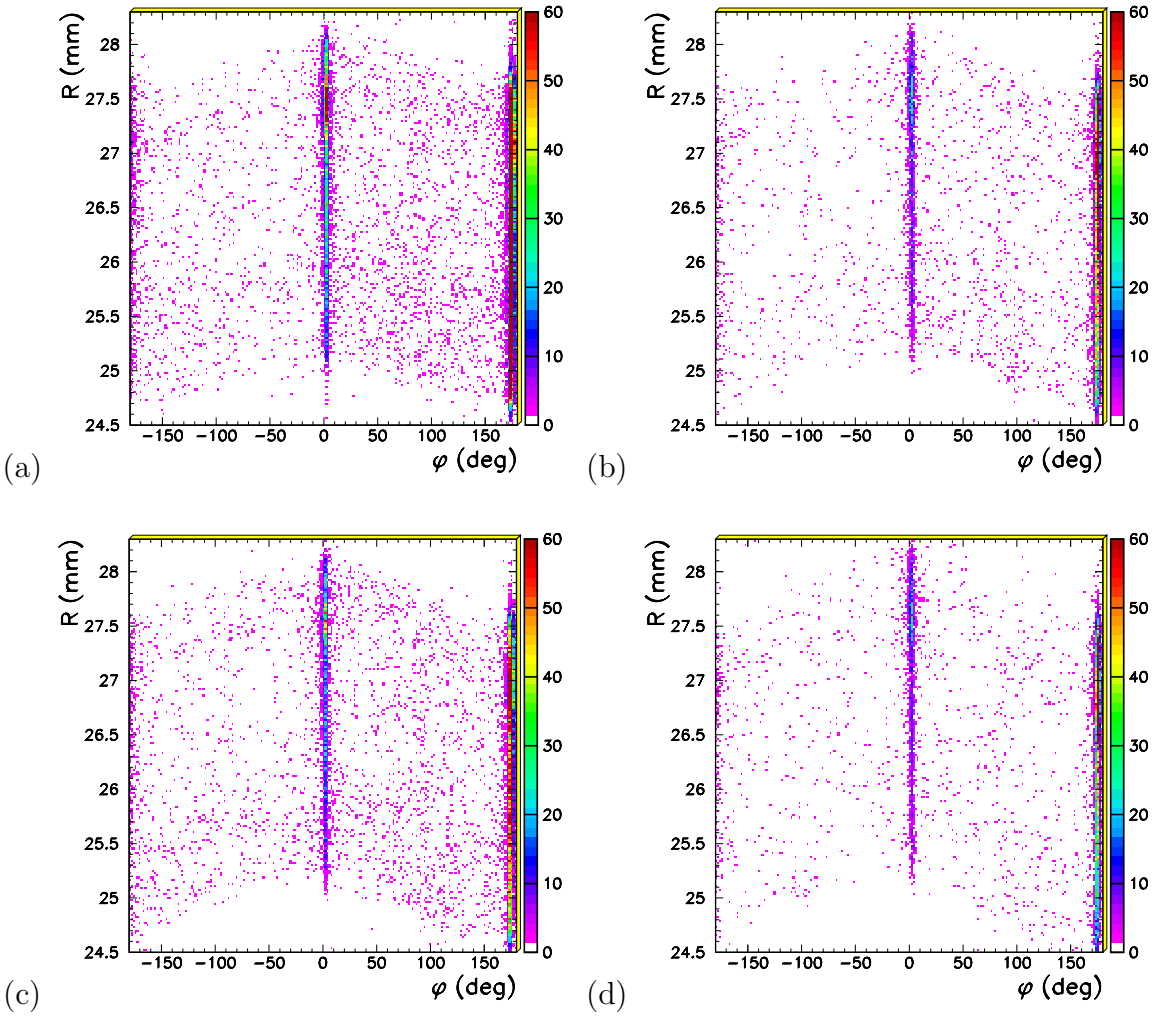

Figure 33: R versus ϕ scatter plots for (a) $-70 < z < 0$ mm, (b) $0 < z < 20$ mm, (c) $20 < z < 50$ mm and (d) $50 < z < 100$ mm.

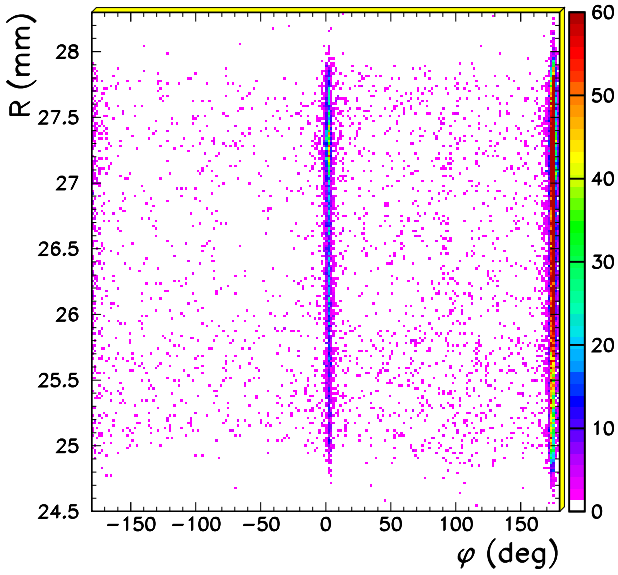

Figure 34: $R(mm)$ versus $\phi(^\circ)$ scatter plot after shift and rotation correction.

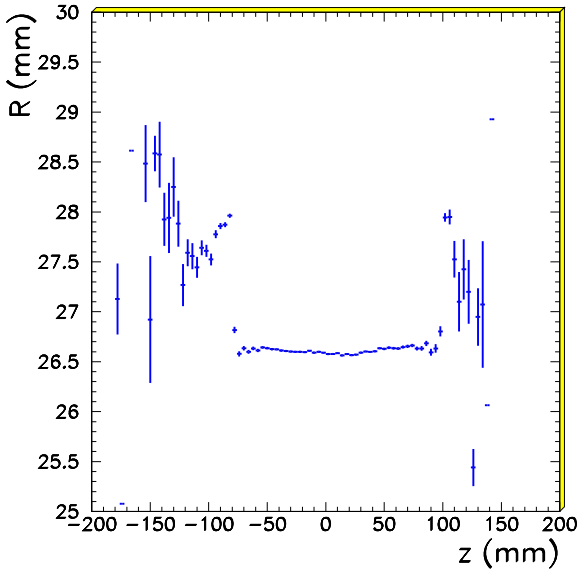

Figure 35: $< R > (mm)$ versus $z(mm)$ profile plot after shift and rotation correction.

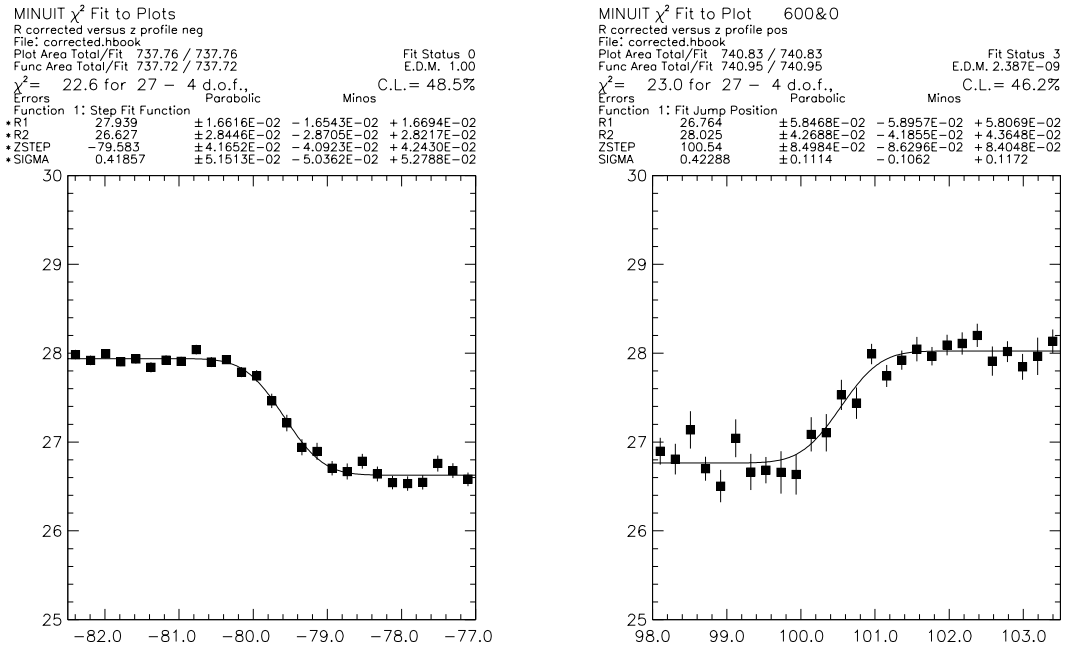

Figure 36: The $< R >$ (mm) versus $z(mm)$ distribution at each end of the beampipe; the curve shows the result of the fit.

References

[1] *BABAR* Analysis Document # 102, The *BABAR* Vertexing.

[2] *BABAR* Analysis Document # 55, Measurement of the Tau Lepton Lifetime with the Decay Lenght Method.

[3] *BABAR* Analysis Document # 83, Measurement of the Tau Lepton Lifetime with the Decay Lenght Method.

[4] $\gamma\gamma \to \pi$: a Control Sample for Vertexing.

[5] G. Raven, $D^{*-} - D^0$ *vertexing in* $B^0 \to D^{*-}\ell\nu$ *events*, talk at $\sin 2\beta$ WorkShop, 3rd November, 2000,
http://www.slac.stanford.edu/BFROOT/www/Physics/CP/beta/Meetings/03Nov00/S2bWorkshop00.html

[6] B. Dunwoodie et al, *BABAR* Analysis Document # 106, Study of material interactions with gamma conversions and protons.

[7] *BABAR* Analysis Document # 130, Vertexing performances and systematic checks with fully reconstructed B events.